NeuroEng 2025 Program

20 – 21 February 2025

Venue: University College - Melbourne Residential College

40 College Cr, Parkville, VIC 3052

Thursday, 20 February 2025

Time	Activity	
9:00 am	Welcome and Keynote Presentation	
	Andre van Schaik	Western Sydney University
10:00 am	Morning Tea	
10:30 am	Oral Presentations	
	Martin Spencer	University of Melbourne
	Lin Liu	University of South Australia
	Rishi Maran	University of Sydney
	Zhuying Chen	University of Melbourne
12:30 pm	Lunch	
1:30 pm	Oral Presentations	
	Leonardo Novelli	Monash University
	Michaela Vranic-Peters	University of Melbourne
	Brendan Harris	University of Sydney
	Colin Hales	University of Melbourne
3:30 pm	Afternoon Tea	
4:00 pm	Poster Session	
6:00 pm	Gala Dinner	

Friday, 21 February 2025

Time	Activity	
9:00 am	Keynote Presentation	
	Ryota Kanai	Arata
10:00 am	Morning Tea	
10:30 am	Oral Presentations	
	Joel Villalobos	University of Melbourne
	Stella Ho	University of Melbourne
	Jieru Liao	University of Sydney
12:00 pm	Lunch	
1:00 pm	Oral Presentations	
	Demi Gao	Bionics Institute
	Wei Qin	University of Melbourne
	Ben Walters	James Cook University
	Yanbo Lian	University of Melbourne
3:00 pm	Afternoon Tea	
3:30 pm	Oral Presentations	
	Manula Somaratna	University of Sydney
	Parvin Zarei Eskikand	University of Melbourne
	Steven Wiederman	University of Adelaide
5:00 pm	Conference Close	

NeuroEng 2025 Program

20 – 21 February 2025

Venue: University College - Melbourne Residential College

40 College Cr, Parkville, VIC 3052

Poster Session, 4:00 pm – 6:00 pm, Thursday, 20 February 2025

Chaerim Kim	Monash University
Daniel Richardson	Swinburne University of Technology
Elnaz Nemati	University of Melbourne
Han Wang	University of Melbourne
Haozhe Wang	Monash University
Jessica Woolley	Monash University
JingYang Liu	University of Melbourne
Kai Sun	Monash University
Kaichao Wu	Monash University
Marko Ruslim	University of Melbourne
Rochelle De Silva	University of Melbourne
Scott Gazzard	University of Melbourne
Stella Ho	University of Melbourne
Suleman Rasheed	University of Melbourne
Toon Goris	University of Melbourne
Weijie Qi	University of Melbourne
Xiaowei Xia	University of Melbourne

Full characterization of high-frequency oscillation networks requires seven days of intracranial EEG recordings

Zhuying Chen[1,2], Stephen V. Gliske[3], Jack Lin[2], Garnett Hegeman[2], David B. Grayden[1*], William C. Stacey[2,4*]
[1] Department of Biomedical Engineering and Graeme Clark Institute, University of Melbourne, Australia.
[2] Department of Neurology, University of Michigan, USA.
[3] Department of Neurosurgery, University of Nebraska Medical Center, USA.
[4] Departments of Neurology and Biomedical Engineering, BioInterfaces Institute, University of Michigan, USA.
[*] Both authors are joint senior authors.
E-mail: zhuying.chen@unimelb.edu.au

High-frequency oscillations (HFOs) in EEG with frequency band above 80 Hz (Figure 1A) is a promising biomarker for identifying seizure focus in drug-resistant epilepsy [1]. Numerous studies have shown that channels with higher HFO occurrence rates often align with the clinically identified seizure onset zone (SOZ). However, most previous studies limited their HFO analysis to short recordings (<30 minutes), which has led to a poor understanding of their spatial and temporal dynamics. Like seizures, the spatial distribution of HFO rates can fluctuate over time (Figure 1B), raising an important but unresolved question: how much data is enough to fully characterize HFO networks?

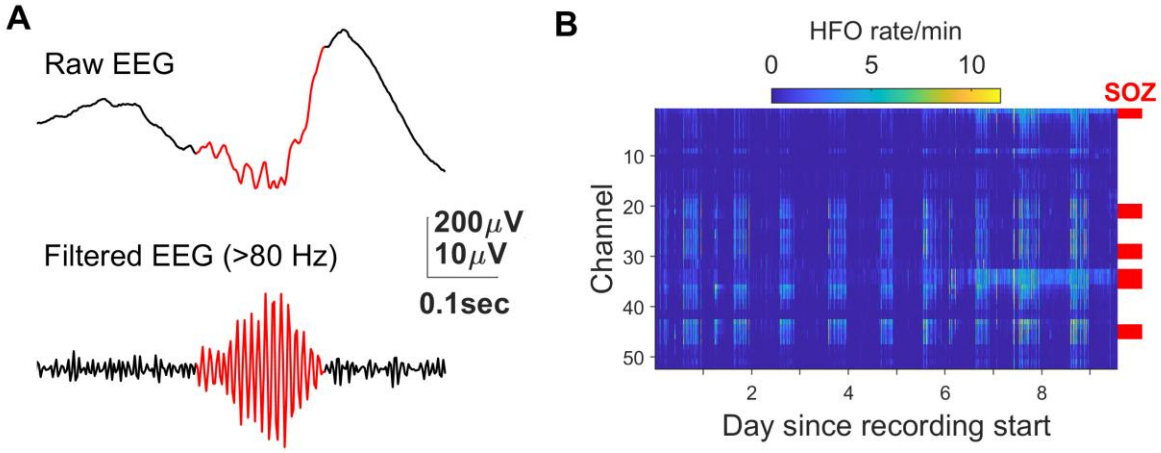

Figure 1. (A) Example of high-frequency oscillations (HFOs). (B). Temporal changes in HFO spatial distribution.

This study presents a novel approach to determining the minimum recording duration required to fully characterize HFO networks. We analyzed long-term, continuous intracranial EEG (iEEG) recordings from 55 drug-resistant epilepsy patients undergoing presurgical evaluation (average duration: 8.32 days per patient). HFOs (80-500 Hz) were automatically detected across the entire recordings using a validated algorithm.

Our findings show that at least 7 days of recordings are required to fully characterize HFO networks in 98% of patients. HFO rates were consistently higher in SOZ channels across all epilepsy types but were more pronounced in temporal lobe epilepsy than in extratemporal lobe epilepsy. Patients with frequent seizures exhibited higher HFO rates and more stable HFO-SOZ correlations.

Our findings suggest that although shorter recordings capture a portion of the HFO network, a minimum of 7 days of data is necessary to account for temporal variability in HFO spatial distributions reliably. Tailoring evaluation strategies based on epilepsy type and seizure frequency may further improve HFO-guided presurgical assessments.

Acknowledgements
This work is supported by the National Institutes of Health [R01-NS094399].

References
1. Chen, Z., Maturana, M. I., Burkitt, A. N., Cook, M. J., & Grayden, D. B. (2021). High-Frequency Oscillations in Epilepsy: What Have We Learned and What Needs to be Addressed. Neurology, 96(9), 439-448.

Rhythmo: A Python toolbox for mapping multiday physiological rhythms and brain dynamics

Rochelle De Silva[1,2], Shivam Puri[1], Rachel E. Stirling[1,2], Jodie Naim-Feil[1,2], Philippa J. Karoly[1,2]
[1] Department of Biomedical Engineering, University of Melbourne, Australia.
[2] Graeme Clarke Institute, University of Melbourne, Australia.

Circadian rhythms encompass 24-hour cycles that govern physiological processes within the body, including sleep-wake patterns and hormone secretion (1). Recent research has increasingly focused on infradian, or multiday rhythms, over longer timescales (e.g., weekly, monthly and seasonal), particularly in the context of epilepsy (2). In addition, multiday rhythms of resting heart rate (measured from wearable devices) were discovered in both people with epilepsy and in healthy individuals, which appeared to be comodulated with cortical excitability (3, 4). Deepening our understanding of multiday rhythms in the general population is crucial, as it can provide insights into the links between our physiology, behavior, and brain dynamics. The onset of wearable devices has allowed for continuous and easy access to rich, long-term datasets and personalized health insights.

Rhythmo is a publicly accessible Python toolbox that extracts individuals' physiological multiday cycles from any long-term datasets (e.g., wearable devices, EEG/ECG and other ExG datasets) and allows for study of longer-term brain dynamics at different phases of these cycles, which have not previously been discerned. Rhythmo provides visualizations (and .csv files) of the dominant physiological cycle and a forecast of the expected future cyclical trend in the data with corresponding sampling times for researchers to schedule participants for brain imaging, brain stimulation and/or behavioral tasks to map how the brain changes along various phases of their cycle. An example application of Rhythmo utilizing heart rate data is displayed in Figure 1.

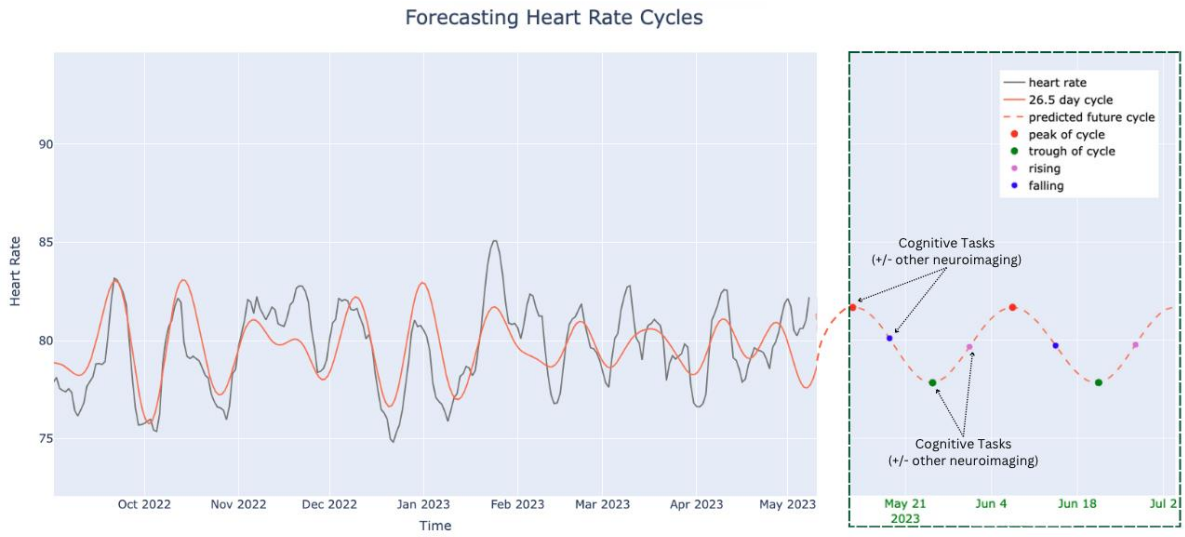

Figure 1. Example heart rate cycle forecast showing historical heart rate data, predicted future cycles, and corresponding sample times (e.g., cognitive tasks with or without other neuroimaging).

Rhythmo is available on GitHub for the public to upload their data and to learn more about their intrinsic rhythms: https://github.com/riplresearch/rhythmo

References

1. Foster RG. Sleep, Circadian Rhythms and Health. Interface Focus. 2020 Apr 17;10(3):20190098.
2. Karoly PJ, Rao VR, Gregg NM, Worrell GA, Bernard C, Cook MJ, et al. Cycles in epilepsy. Nature Reviews Neurology. 2021 Mar 15;17(5):267–84.
3. Gregg NM, Tal Pal Attia, Nasseri M, Joseph B, Karoly PJ, Cui J, et al. Seizure occurrence is linked to multiday cycles in diverse physiological signals. Epilepsia. 2023 Apr 20;64(6):1627–39.
4. Karoly PJ, Stirling RE, Freestone DR, Nurse ES, Maturana MI, Halliday AJ, et al. Multiday cycles of heart rate are associated with seizure likelihood: An observational cohort study. EBioMedicine. 2021 Oct 1;72:103619.

Measuring speech discrimination ability in sleeping infants using fNIRS

Demi X. Gao[1, 2], Onn Wah Lee[3], Tommy Peng[1, 2], Julia Wunderlich[1, 2], Darren Mao[1, 2], Gautam Balasubramanian[1, 2], Colette M. McKay[1, 2]

[1] Bionics Institute, Daly Wing, St Vincent's Hospital, Level 7, 35 Victoria Parade, Fitzroy VIC 3065.

[2] Department of Medical Bionics, University of Melbourne, Parkville, VIC 3010, Australia.

[3] Centre for Rehabilitation & Special Needs Studies, Faculty of Health Sciences, University Kebangsaan Malaysia, 50300 Kuala Lumpur, Malaysia.

E-mail: dgao@bionicsinstitute.org

This study used functional near-infrared spectroscopy (fNIRS) to measure the speech discrimination ability of sleeping infants. Speech discrimination refers to the ability to differentiate between different speech sounds. We examined the morphology of the fNIRS response to three different speech contrasts, namely "Tea/Ba", "Bee/Ba" and "Ga/Ba". Sixteen infants aged between 3 and 13 months old were included in this study and their fNIRS data were recorded during natural sleep. The stimuli were presented using a non-silence baseline paradigm, where repeated standard stimuli were presented between the novel stimuli blocks without any silence periods. The morphology of fNIRS responses varied between speech contrasts. The data were fitted with a model in which the responses were the sum of two independent and concurrent response mechanisms that were derived from previously published fNIRS detection responses [1]. These independent components were a HbO-positive early-latency response and a HbO-negative late latency response, hypothesised to be related to auditory canonical response and brain arousal response, respectively. The goodness of fit of the model with the data was high with median goodness of fit of 81%. The data showed that responses of both response components had longer peak latencies when the left ear was the test ear ($p<0.05$) compared to the right ear. The negative component, due to brain arousal, was smallest for the most subtle contrast, "Ga/Ba" ($p = 0.003$). Further research is needed in larger groups of infants with both normal and impaired hearing to confirm these results and to investigate how these findings might be applied in individual infants to provide clinically-relevant information.

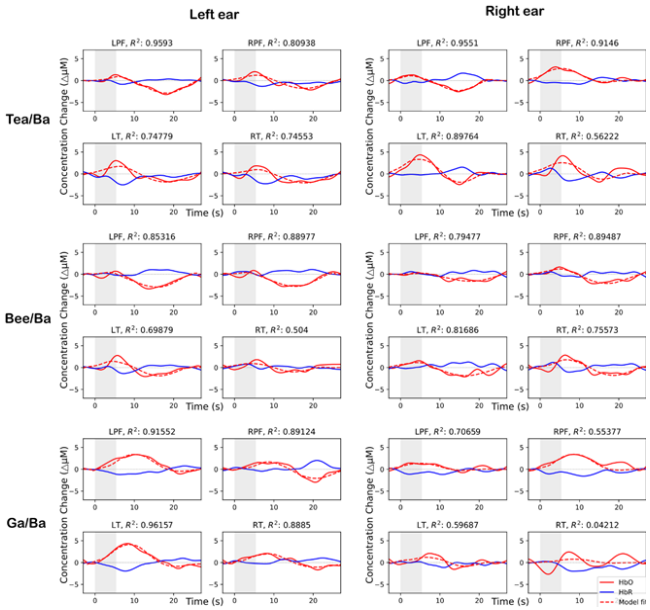

Figure 1. HbO (solid red lines) and HbR (solid blue lines) waveforms, averaged across subjects. The left and right columns are results from infants with left and right ear stimulation, respectively and rows are results for the three different speech contrasts. The dashed red lines are model fits to the HbO data. LPF, RPF signify left and right prefrontal Regions of Interest (ROIs) respectively, and LT, RT signify left and right temporal ROIs respectively.

Acknowledgements

The authors would like to thank the Victorian Infant Hearing Screening Program (VIHSP) for its support in participant recruitment. The first author is funded by a Garnett Passe and Rodney Williams Memorial Foundation Mid-Career Fellowship. This project was supported by The HHMRC (GNT1154233), and MTPConnect (EarGenie BMTH 03), the Victorian Medical Research Acceleration Fund and the Garnett Passe and Rodney Williams Memorial Foundation. The Bionics Institute acknowledges the support it receives from the Victoria State Government through its Operational Infrastructure Support Program.

References

[1] Lee, O. W., Mao, D., Wunderlich, J., Balasubramanian, G., Haneman, M., Korneev, M., & McKay, C. M. (2024). Two independent response mechanisms to auditory stimuli measured with fNIRS in sleeping infants. Trends in Hearing 28: 1-11. doi: 10.1177/23312165241258056.

[2] Lee, O. W., Gao, D, Peng, T., Wunderlich, J., Mao, D., Balasubramanian, G., & McKay, C. M. (2024). Measuring speech discrimination ability in sleeping infants using fNIRS – a proof of principle. Trends in Hearing, accepted. doi: 10.1177/23312165241311721.

The Propagating Wavefront Identity network as a model for associative learning in the brain

Scott Gazzard[1], Yanbo Lian[1], Anthony N. Burkitt[1], Hamish Meffin[1]
[1] Department of Biomedical Engineering, The University of Melbourne, Australia.
Email: scott.gazzard@student.unimelb.edu.au

This presentation introduces a novel neural network architecture that aims to provide a biologically plausible model for information transmission and associative learning in the animal brain. The Propagating Wavefront Identity (PWI) network model involves a Spiking Neural Network comprising one or more 2-dimensional layers of Leaky Integrate-and-Fire neurons with nearest-neighbour synaptic connections. The network architecture results in the propagation of spreading wavefronts of neural activation across the surface of each neural layer (see Figure 1A). The wavefronts originating from different stimulus locations on the neural layer exhibit unique spatiotemporal properties, including radius and orientation, as they propagate. It is posited that the unique spatiotemporal properties of propagating wavefronts can be recognised by response neurons that are distant from the stimulus origin, without any direct or near-direct connections existing between the stimulus and response (see Figure 1B). The response neurons act as feature detectors that respond to a particular wavefront's spatiotemporal properties (its "identity") and thus the response neuron can be said to be responding to the distant stimulus activation.

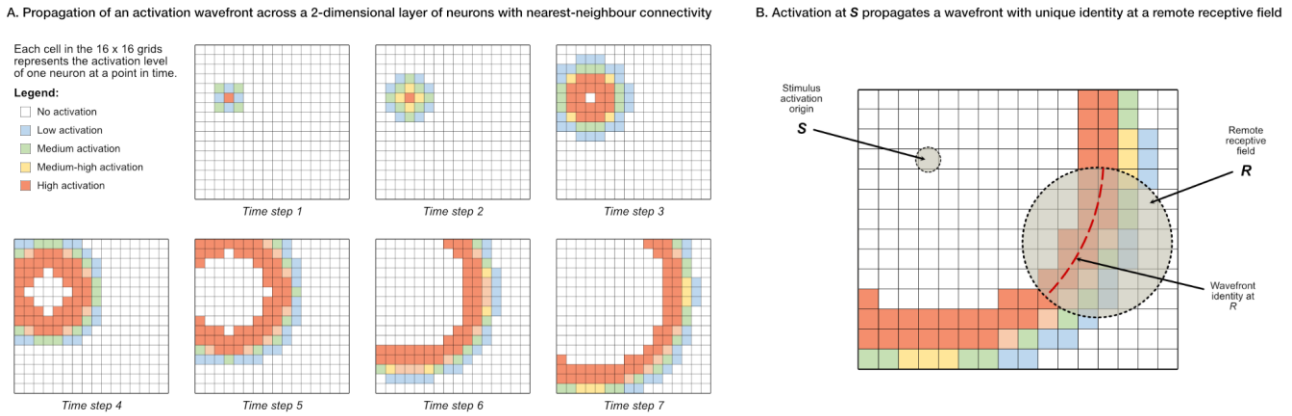

Figure 1. A) Propagation of an activation wavefront across a 2-dimensional layer of neurons. Each neuron that fires tends to activate its nearest neighbours, which in turn activate their nearest neighbours, and so on. A brief refractory period prevents reactivation after spiking to ensure that the wavefront only travels in one direction. B) Activation of a stimulus neuron at position *S* on the neural layer propagates an activation wavefront which can be recognised by its unique radius and orientation at point *R*.

Response neurons have a set of afferent connections that are activated by neurons in a local region of the 2-dimensional neural layer (the neuron's "receptive field") and can either possess a pattern of connections that predispose them to respond to particular wavefront identities, or they can modify their connection strengths to learn to respond to particular identities. Learning to identify and respond to wavefront identities only involves synaptic modification of the afferent connections of the response neuron (utilising biologically inspired methods such as Spike-Timing-Dependent Plasticity [STDP]), and so avoid the need for algorithms such as backpropagation of error. Training of such networks can be unsupervised or may involve the application of reinforcement learning techniques in conjunction with STDP to shape the network's responses. Simple versions of the network allow for learning of simple associations between single stimulus and response pairs; however, it is proposed that more complex versions of the network, which involve multiple neural layers and the propagation of multiple simultaneous activation wavefronts, may enable the learning of far more complex associations. Preliminary results from *in silico* experiments involving simple forms of the PWI network architecture will be provided in the presentation.

Modulation of mechanosensitive retinal ganglion cells using high frequency focused ultrasound

Toon Goris[1], Jack Drummond[2], Negar Zoka[2], Kalyan Shobhana[3], Han Wang[1], Rachael Richardson[4], Melanie Stamp[2], David Collins[2], Michael R. Ibbotson[2], Sam John[2], Wei Tong[1]
[1] Department of Physics, University of Melbourne, Parkville, Australia.
[2] Department of Biomedical Engineering, University of Melbourne, Parkville, Australia.
[3] Biological Optical Microscopy Platform, The University of Melbourne, VIC, Australia
[4] Department of Medical Bionics, University of Melbourne, Parkville, Australia.
E-mail: toon.goris@unimelb.edu.au

Vision loss due to the degeneration of light-sensitive cells in the retina significantly reduces the quality of life for patients with retinal degenerative diseases such as retinitis pigmentosa (1/4000 people affected) and age-related macular degeneration (8% population affected). Current research efforts aim to restore vision in these patients using retinal prostheses, which bypass the damaged light-sensitive layer and directly transmit visual information to the intact retinal ganglion cells. Approaches include electrical stimulation of retinal ganglion cells or optical stimulation of genetically modified ganglion cells. Although these methods show promise, they are invasive and lack the ability to build upon the residual vision of the patient, respectively.

Our study explores an alternative approach involving mechanical stimulation of retinal ganglion cells using high-frequency ultrasound waves. Retinal ganglion cells are not inherently responsive to mechanical stimuli and must be genetically modified to express mechanosensitive ion channels (Figure 1). Previous studies have shown that the expression of mechanosensitive ion channels in retinal ganglion cells can render these cells sensitive to ultrasound stimuli with a frequency-dependent spatial resolution.[1]

In this study, we used focused ultrasound waves in an ex vivo animal model (RCS-P+) to assess the effects on genetically modified mechanosensitive retinal ganglion cells. Our results demonstrate that high frequency ultrasound stimulation can effectively modulate the frequency and amplitude of cell activity. This study provides proof of concept for the use of high frequency ultrasound stimulation in novel retinal prosthetics modulating retinal ganglion cell activity and improving the quality of life in visually impaired patients suffering from retinal degenerative diseases.

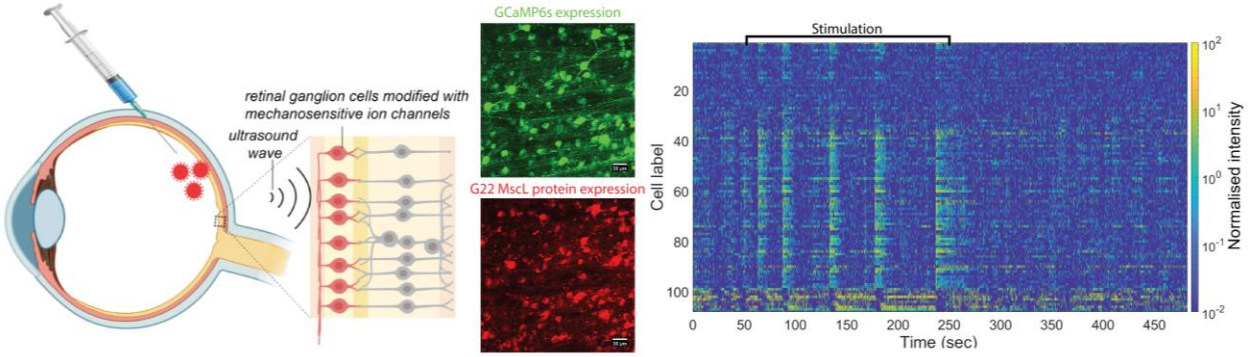

Figure 1. Transduction of the ion channel DNA to the retinal ganglion cells using AAV vectors (left) is followed by fluorescence calcium imaging of the dissected RCS-P+ retina. The fluorescence originating from the GCaMP6s calcium indicator is shown in green while the expression of the mechanosensitive ion channel, G22 MscL, is shown in red. The fluorescence intensity over time for each cell is deconvoluted and displayed in a rasterplot (right). A shift in action potential frequency and amplitude is observed during the stimulation window.

Acknowledgements
Research was funded by the National Health and Medical Research Council (NHMRC) Ideas Grant. [2029454]

References
1.Cadoni, S., et al., *Ectopic expression of a mechanosensitive channel confers spatiotemporal resolution to ultrasound stimulations of neurons for visual restoration.* Nature Nanotechnology, 2023. **18**(6): p. 667-676.

The Neuromimetic Chip: Introduction, Progress update, Outlook

Colin G. Hales[1]
[1] Department of Anatomy and Physiology, University of Melbourne, Australia.
E-mail: cghales@unimelb.edu,au

The neuromimetic chip is a design concept for robotic machine intelligence in the form of the nervous system of robots that learn like natural fauna learns. The nervous system technology is best thought of as inorganic reverse-engineered excitable cell tissue. This physics-replication approach involves no abstract models of brain tissue physics or function. Instead of the physics of a general-purpose computer or the physics of abstract models of the brain (analogue or digital), a neuromimetic chip has an inorganic version of natural adaptive brain signaling physics. That is, it is literally based on the identical causality found in natural brain tissue. Fully developed at macroscopic scales it can be expected to produce an EEG/MEG-like electromagnetic signature. The neuromimetic chip fits as a member of the class of "in-materio" unconventional computing, where the "in-materio" part is nervous signaling rendered inorganically. In the context of the central nervous system, the chip is intrinsically an "edge-of-chaos" processor based on the electromagnetic field phenomena created by membranes penetrated by ion channels. The neuromimetic approach is currently completely missing from the science. The conceptual basis of the chip is demonstrated to be a correction (a normalization) to a science distorted at the birth of AI in 1956. To illustrate the current state of the development of the chip, we reveal the prototyping that has produced a macroscopic (roughly 20,000x) version of a small patch of membrane penetrated by a single "ion channel". The intent is to explore, at macroscopic scale, the causal origins of the cusp leading to chaotic stability. This is designed to discover the minimum number of devices and the topology needed to express the rudimentary symmetry breaking needed for autonomous learning. While it is early days, and the next stages are unfunded, and the deep-tech fabrications challenges are extreme, the approach is on untrodden ground and shows great promise in dealing with the well-known limitations of current machine intelligence approaches.

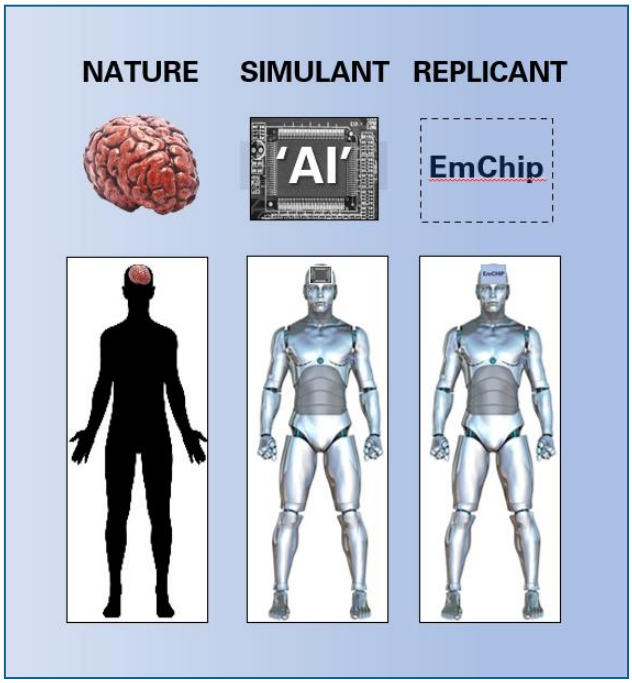

References

Colin G. Hales. **The Model-less Neuromimetic Chip and its Normalization of Neuroscience and Artificial Intelligence**. TechRxiv. February 08, 2021. DOI: 10.36227/techrxiv.13298750.v4
https://www.techrxiv.org/doi/full/10.36227/techrxiv.13298750.v4%20 (2 supplementary, 5 videos).

Nested spatiotemporal theta–gamma waves organize hierarchical visual processing

Brendan Harris, Pulin Gong
School of Physics, The University of Sydney, Camperdown NSW, Australia
bhar9988@uni.sydney.edu.au

Neural dynamics bridge anatomy and function over diverse scales [1], from microscopic spiking to mesoscale LFPs [2] and macroscopic traveling waves [3, 4, 5]. We report a new nested dynamical pattern in the mouse visual cortex, comprising: i) large-scale θ waves that propagate across cortical layers and regions; ii) short, localized γ packets that reflect focused processing; and iii) cross-scale coupling between θ waves, γ packets, and spikes (illustrated in Fig. 1A). This flexible dynamical motif aligns with feed-forward/feed-back anatomical features of the visual hierarchy and cortical laminae, while also carrying significant top-down/bottom-up functional information that predicts change-detection performance. Our findings suggest that such distributed cross-scale patterns form a general 'spatiotemporal θ–γ code' for efficiently modulating and multiplexing neural information.

We used wave-based methods to analyze the 'Allen Neuropixels–Visual Behavior' dataset, illustrated in Fig. 1B, which comprises multi-region laminar recordings from the mouse visual cortex. After systematically mapping local field potential spectra to identify dominant timescales, we characterized θ as a traveling wave using the instantaneous phase (Fig. 1D) and quantified translaminar propagation with the negative spatial phase gradient (see Fig. 1E). We then used the instantaneous amplitude to detect non-stationary, spatially localized γ packets across layers (Fig. 1F). Finally, by extended classical phase–amplitude coupling measures, we detected spatiotemporal θ–γ interactions that coordinate large-scale traveling θ waves with localized γ packets (illustrated in Fig. 1G) and neuronal spiking.

All regions exhibited clear θ-band (3–$10\,\mathrm{Hz}$) and γ-band (30–$100\,\mathrm{Hz}$) peaks. We also discovered a robust spectral gradient along the visual cortical hierarchy [6], with θ strength increasing toward deep layers (median Kendall's $\tau = 0.37$, $p < 10^{-7}$) and higher regions ($0.25 < \tau < 0.60$ across layers, all $p < 0.01$). θ displayed striking bidirectional, nonstationary propagation during visual tasks, switching from a deep-to-superficial feed-back mode after onset to a superficial-to-deep feed-forward mode after offset. θ also propagated from higher to lower areas near stimulus onset, but in the reverse direction following offset. Furthermore, translaminar θ propagation (prior to reaction) predicted 'hit/miss' change-detection performance, with a balanced accuracy of 0.65 ± 0.11 (median $\pm$ IQR across sessions, 5 folds, 20 repeats, $p < 10^{-13}$). Together, these results indicate that θ plays a dual functional role in visual cognition.

γ, on the other hand, formed spatiotemporal wave packets, which became spatially localized after stimulus onset. γ packets were also locked to θ waves, particularly in layer 1 of lower-order areas and layer 6 of higher-order regions. Moreover, γ packets in superficial layers tended to prefer θ troughs, whereas deep layers preferred the falling edge. This θ–γ locking was mirrored in the relationship between LFP and neuronal spiking, where spikes tracked fluctuations in γ power and exhibited similar layer-specific preferences of θ phase.

Based on our findings, we introduce a spatiotemporal θ–γ code that provides a general mechanism for multiplexing and integrating fine-grained top-down and bottom-up information across cortical layers and brain regions. Our wave-based framework ties local cross-scale coupling [7] and inter-areal phase synchrony [8] into a coherent, nested pattern of neuronal spiking, γ packets, and θ traveling waves, highlighting the crucial role of large-scale dynamics in shaping the fine-grained processes needed to interpret complex natural stimuli.

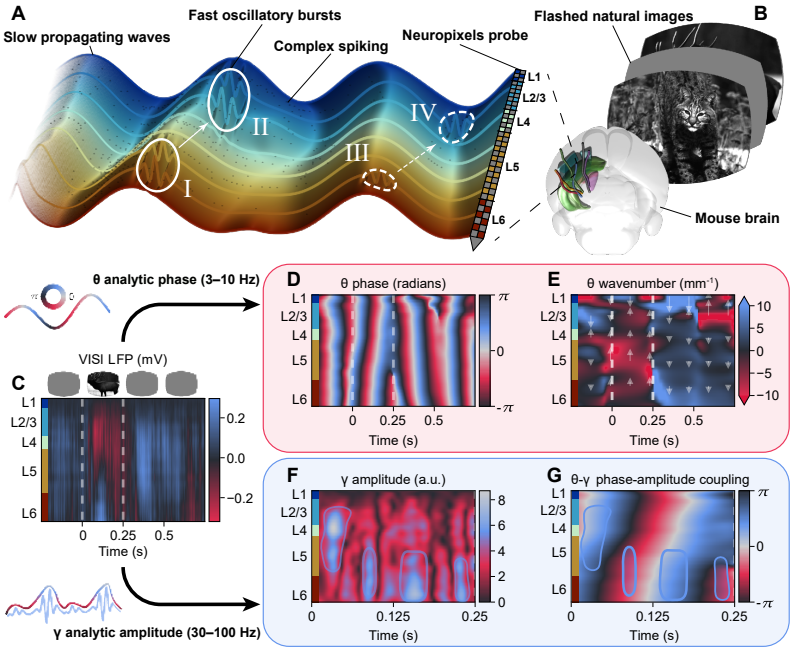

Figure 1: A schematic of the spatiotemporal θ–γ code and our methods for detecting nested spatiotemporal patterns.
(A) A spatiotemporal θ–γ code describes how slow traveling waves (solid surface) and high-frequency packets (circled) can modulate and multiplex distributed neural information. Packet I represents strong activation in deep layers, coinciding with a traveling θ wave that meets II at a peak, enhance superficial γ. Conversely, packet III represents weak activity in deep layers coinciding with a stationary θ wave, meaning packet IV occurs at a θ trough and is suppressed.
(B) We studied LFP and spike data from the mouse visual cortex during image viewing.
(C) Representative single-trial LFPs in `VISl`, shown across time and cortical layers (blue to red bars, left).
(D) θ analytic phases reveal translaminar propagating patterns.
(E) The negative spatial phase gradient quantifies θ propagation; positive (negative) values indicate downward (upward) propagation.
(F) The analytic amplitude of γ highlights localized packets of activity (circled blue).
(G) γ packets are nested inside θ traveling waves.

References

[1] Senkowski et al., *Multi-timescale neural dynamics for multisensory integration*, Nat. Rev. Neurosci. **25**, 625–642 (2024).

[2] Hayden et al., *Electrophysiological signatures of visual recognition memory across all layers of mouse v1*, J. Neurosci. **43**, 7307–7321 (2023).

[3] Townsend et al., *Detection and analysis of spatiotemporal patterns in brain activity*, PLoS Comput. Biol. **14**, e1006643 (2018).

[4] Aggarwal et al., *Visual evoked feedforward-feedback traveling waves organize neural activity across the cortical hierarchy in mice*, Nat. Commun. **13**, 4754 (2022).

[5] Xu et al., *Interacting spiral wave patterns underlie complex brain dynamics and are related to cognitive processing*, Nat. Hum. Behav. **7**, 1196–1215 (2023).

[6] Siegle et al., *Survey of spiking in the mouse visual system reveals functional hierarchy*, Nature **592**, 86–92 (2021).

[7] Senzai et al., *Layer-specific physiological features and interlaminar interactions in the primary visual cortex of the mouse*, Neuron **101**, 500–513.e5 (2019).

[8] Liebe et al., *Theta coupling between v4 and prefrontal cortex predicts visual short-term memory performance*, Nat. Neurosci. **15**, 456–462 (2012).

Visual decoding from intracranial recordings using deep learning

Stella Ho[1,2], Joel Villalobos[1,2], Joseph West[3], Takufumi Yanagisawa[4], Sam E. John[1,2], David B. Grayden[1,2]
[1] Department of Biomedical Engineering, University of Melbourne, Victoria, Australia.
[2] Graeme Clark Institute for Biomedical Engineering, University of Melbourne, Victoria, Australia.
[3] School of Computing and Information Systems, University of Melbourne, Victoria, Australia
[4] Department of Neurosurgery, Graduate School of Medicine, Osaka University, Suita, Japan
E-mail: stella.ho@unimelb.edu.au

Deep learning models have shown promise in neural decoding, given their flexibility and adaptability in high-dimensional data analysis. In this study, we explored deep learning models as neural encoders for classifying colour stimuli from the sheep primary visual cortex. The challenges with this visual decoding task included limited number of events per experimental session per animal and the fact that sheep are green-red colourblind. To address this, the classification labels were designed with ON/OFF stimulus states for green, red and blue stimuli. As a result, the task was to decode neural responses into one of these six classes.

To tailor the model complexity to the dataset size, the choice of the neural networks was narrowed down to simple yet effective neural networks, including multi-layer perceptron [1], convolutional neural networks (CNN) [2] with 1-dimensional kernels (1D CNN) and 2-dimensional kernels, long short-term memory networks [3], gated recurrent units [4] and auto-encoder [5]. The results showed that 1D CNN outperformed other models, achieving an average accuracy of 69.3% across the five sheep. This performance was notable given that 1D CNN was trained on only 480 samples per sheep. In addition, various signal representations, i.e., raw signal, spectrogram and trimmed spectrogram, were analysed as inputs for these models. The result showed that raw signals were the most robust inputs, aligning with findings reported in recent literature [6, 7]. This is as expected, as deep learning models are able to automatically capture underlying features from raw signal without the need of explicit feature engineering.

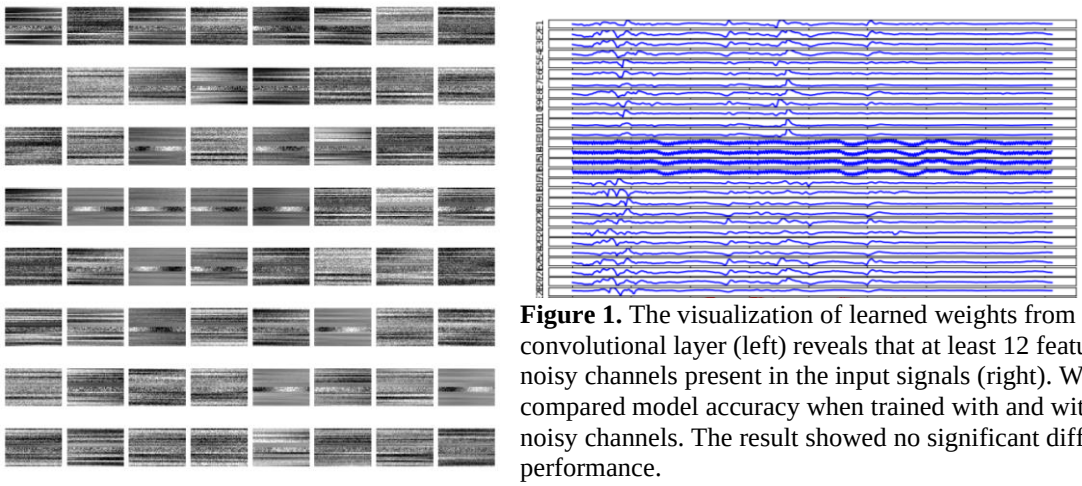

Figure 1. The visualization of learned weights from the first convolutional layer (left) reveals that at least 12 feature maps detect noisy channels present in the input signals (right). We then compared model accuracy when trained with and without these noisy channels. The result showed no significant difference in performance.

Acknowledgements
This research was funded by the Japan Science and Technology Agency (JST) Moonshot R&D (JPMJMS2012).

References

1. Haykin S.: **Neural networks: a comprehensive foundation.** *Prentice Hall PTR*; 1994.
2. LeCun Y, Bengio Y, Hinton G.: **Deep learning.** *Nature.* 2015 May 28;521(7553):436-44.
3. Hochreiter, S. and Schmidhuber, J.: **Long Short-Term Memory.** *Neural Computation* 1997, 9(8):1735-1780.
4. Cho, K., Van Merriënboer, B., Gulcehre, C., et al.: **Learning Phrase Representations using RNN Encoder-Decoder for Statistical Machine Translation.** *arXiv* 2014, arXiv:1406.1078
5. Baldi P.: **Autoencoders, unsupervised learning, and deep architectures.** *In Proceedings of ICML Workshop on Unsupervised and Transfer Learning* 2012 Jun 27 (pp. 37-49).
6. Van Putten MJ, Olbrich S, Arns M.: **Predicting sex from brain rhythms with deep learning.** *Scientific Reports.* 2018 Feb 15;8(1):3069.
7. Siddhad G, Gupta A, Dogra DP, Roy PP.: **Efficacy of transformer networks for classification of EEG data.** *Biomedical Signal Processing and Control.* 2024 Jan 1;87:105488.

Visual semantic decoding from electrocorticography via large language models

Stella Ho[1,2], Joel Villalobos[1,2], Joseph West[3], Takufumi Yanagisawa[4], Sam E. John[1,2], David B. Grayden[1,2]
[1] Department of Biomedical Engineering, University of Melbourne, Victoria, Australia.
[2] Graeme Clark Institute for Biomedical Engineering, University of Melbourne, Victoria, Australia.
[3] School of Computing and Information Systems, University of Melbourne, Victoria, Australia
[4] Department of Neurosurgery, Graduate School of Medicine, Osaka University, Suita, Japan
E-mail: stella.ho@unimelb.edu.au

Visual semantic decoding in neuroscience refers to the process of translating visual information into semantic concepts or representations through brain activity. This topic of research is imperative to uncover how brain neural activity correlates with semantic concepts and has potential to revolutionize the way we communicate, especially in the field of brain-computer interfaces (BCIs). In this study, we explore decoder-only large language models (LLMs), such as GPT [1], in the context of visual semantic decoding from electrocorticography (ECoG), particularly focusing on open-vocabulary decoding.

A subject-specific model was developed to investigate the feasibility of semantic decoding from visual pathways using LLMs. Specifically, we employ encoder-decoder architecture, which consists of a neural encoder and a pre-trained LLM, i.e., GPT-2.0. The neural encoder maps the ECoG data into high-level neural representations, while the decoder interprets the neural representations into natural language. In this work, we use three distinct encoders: (1) a 1D convolutional neural network (CNN) [3], (2) a customized transformer [4] encoder that jointly attends to both spatial and temporal dimensions, and (3) a simplified transformer encoder with causal attention.

The ECoG recordings were collected from a subject in Japan with drug-resistant epilepsy [2]. The neural responses were recorded while the subject watched six 10-minute videos and four repeated 2.5-min video. These videos were then segmented at 1 s intervals, resulting in a total of 3,750 non-overlapping frames. Five native speakers of Japanese manually annotated 3,750 frames.

In the experiment, we trained the models on 3,000 signal-text training pairs, assessing their performance on 750 test samples. However, the generated text is fragmented and ungrammatical. Thus, we post-processed the output by removing stop words and calculating the overlap of non-stop words (informative terms) between generated and reference texts. 1D CNN slightly outperformed the other two transform-based neural encoders. The result of 1D CNN demonstrated that 99.2% of test samples contain at least one informative word, while 45.7% contain at least five informative words. Additionally, the ROUGE-1score and BERTScore without removing the stop words from the generation were 28.2% and 38.3, respectively.

Overall, these results indicate a reasonable but not high lexical overlap and semantic similarity between the model output and the reference text. One possible reason for this is the difference in interpretation of the same visual information between subject and annotators.

Acknowledgements
This research was funded by the Japan Science and Technology Agency (JST) Moonshot R&D (JPMJMS2012).

References
1. Radford A, Wu J, Child R, Luan D, Amodei D, Sutskever I. **Language models are unsupervised multitask learners.** *OpenAI blog.* 2019 Feb 24;1(8):9.
2. Fukuma R, Yanagisawa T, Nishimoto S, Sugano H, Tamura K, Yamamoto S, Iimura Y, Fujita Y, Oshino S, Tani N, Koide–Majima N.: **Voluntary control of semantic neural representations by imagery with conflicting visual stimulation.** *Communications Biology.* 2022 Mar 18;5(1):214.
3. LeCun Y, Bengio Y, Hinton G.: **Deep learning.** *Nature.* 2015 May 28;521(7553):436-44.
4. Vaswani A. **Attention is all you need.** *Advances in Neural Information Processing Systems*. 2017.

Effect of Temperature on Spiking Activity in an In Vivo Animal Model

Mahdi M. Hussaini[1], Bernard J. E. Evans[2], David C. O'Carroll[3] and Steven D. Wiederman[1#]
[1]School of Biomedicine, The University of Adelaide, Australia
[2]School of Computer Science, The University of Adelaide, Australia
[3]Lund University, Sweden
#Email: steven.wiederman@adelaide.edu.au

Dragonflies experience highly varied head temperatures when foraging in the wild (Figure 1). Biochemical processes, including those underlying neuronal processing, are affected by such changes in temperature[1]. For decades, the dragonfly brain has been used as a model system to understand neuronal processing. From this understanding, we have developed neuro-inspired models of target-detection and tracking, translating these models to hardware platforms.

Although they have a relatively small brain (< 2 million neurons), dragonflies perform complex behaviours, such as pursuing small moving prey and conspecifics. A class of neurons referred to as 'Small Target Motion Detectors' (STMD) are likely to underlie this remarkable hunting ability. STMD responses are tuned to both the size and velocity of dark targets presented to the dragonfly[2]. However, these neuronal responses have typically been studied in controlled environments (temperature of ~25 degrees). Here we investigated how a realistic range of head temperatures affects the physiological properties of these neurons.

Temperatures dramatically altered neuronal responses inducing a large 8.7-fold increase in the contrast sensitivity of STMD neurons (Figure 2A). Intriguingly, size-tuning remained the same with suppression of responses to larger targets unaltered (Figure 2B). Not only was the optimum of velocity tuning increased, but the fastest velocities encoded were extended by an order of magnitude (data not shown).

Our findings emphasize the importance of controlling the temperature in laboratory environments. The results raise new questions about how information is represented within the brain of these flying insects, given the relationship between target parameters (size, velocity) with neuronal activity varies so dramatically depending on current environmental conditions.

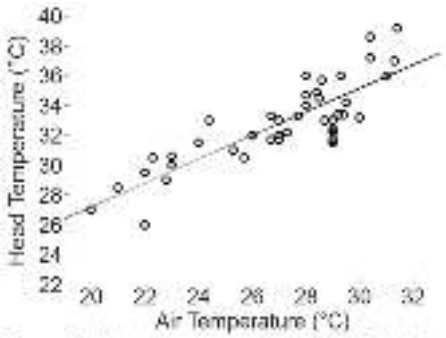

Figure 1: Head temperatures of Hemicordulia tau recorded by rapid insertion of a thermocouple into head capsules of freshly caught dragonflies under a range of ambient conditions (N=43 dragonflies)

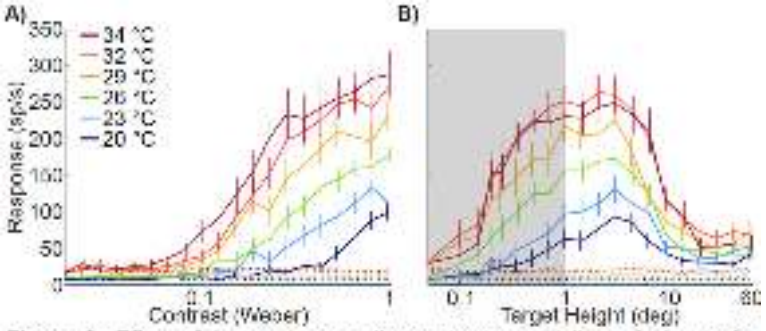

Figure 2: Effect of temperature on the contrast sensitivity and size tuning for moving features (dotted lines = spontaneous). (A) Contrast was varied for 1.5° x 1.5° targets moved at 60°/s (N=11-20). (B) Response to high contrast, fixed width (1.5°) targets with varying heights. Here we see that this increased sensitivity permits detection of smaller features at higher temperatures (shaded area), while there is no apparent effect on lateral inhibition induced by larger objects (N=13-22).

References

[1] Ruoff, P., et al. (2007). "Temperature compensation through systems biology." The FEBS Journal 274(4): 940-950.
[2] Wiederman, S. D. and O'Carroll, D. C. (2011). "Discrimination of features in natural scenes by a dragonfly neuron." The Journal of neuroscience 31(19): 3) 7141-7144.

Evaluating Directional Perception Through Wrist Vibration for Vision Impaired Individuals

Chaerim Kim[1], José Argañarás[1], Yan T. Wong[1,2]
[1] Department of Electrical and Computer Systems Engineering, Monash University, Clayton, VIC, Australia
[2] Department of Physiology and Biomedicine Discovery Institute - Neuroscience Program, Monash University, Clayton, VIC, Australia.
E-mail: chaerim.kim@monash.edu

Wrist-worn tactile displays are proposed to be effective for enhancing mobility in individuals with visual impairments, leveraging the high sensitivity of the wrist to vibrotactile stimulation[1]. These devices offer hands-free convenience, beneficial for visually impaired pedestrians. However, current systems face limitations in spatial resolution and the complexity of tactile stimuli, restricting their ability to convey rich directional information. This study investigated the effects of motor configurations (4-motor vs. 8-motor) and feedback designs (single-motor vibration, dual-simultaneous vibration, and dual-sequential vibration) on directional perception, aiming to overcome these challenges.

Methodology

A wristband prototype with eight eccentric rotating mass motors was developed, enabling 4-motor and 8-motor configurations. Motors were placed at specific angles on the wrist: 0°, 90°, 180°, and 270° for the 4-motor setup, with additional positions at 45°, 135°, 225°, and 315° for the 8-motor setup. Feedback modes included single vibration, where one motor vibrates; dual simultaneous, where two motors vibrate concurrently; and dual sequential, where two motors vibrate in sequence. Vibration intensity (Pulse Width Modulation) was modulated to represent finer angular distinctions. Participants wore the wristband on their left wrist and recorded perceived vibration directions by clicking on a circular protractor displayed on a screen.

Results

In the 4-motor configuration, participants achieved higher motor recognition accuracy (87.5%) compared to the 8-motor setup (61%). Among feedback modes, single vibration mode had the highest accuracy (93.4%) and the fastest response times (1.8 seconds), while dual sequential mode showed the best angular precision with the lowest error (11.6°). The 8-motor configuration demonstrated slightly better angular accuracy overall (23.2° vs. 29.7° for 4-motor) but showed minimal differences across feedback modes in both recognition accuracy and error. Response times in the 8-motor setup were similar but slightly faster overall.

These findings suggest that the 4-motor configuration provides an optimal balance of simplicity and performance. Single vibration mode offers intuitive and fast feedback, while dual sequential mode improves angular precision. Future work will refine vibration patterns for the 4-motor configuration and extend evaluations to three-dimensional tasks for enhanced directional guidance.

References

[1] R. Tapu, B. Mocanu, and T. Zaharia, “Wearable assistive devices for visually impaired: A state of the art survey,” *Pattern Recognit. Lett.*, vol. 137, pp. 37–52, Sep. 2020, doi: 10.1016/j.patrec.2018.10.031.

Learning egocentric spatial cells in the postrhinal cortex

Yanbo Lian[1], Anthony N. Burkitt[1,2],
[1] Department of Biomedical Engineering, University of Melbourne, Parkville, Australia
[2] Graeme Clark Institute, University of Melbourne, Parkville, Australia
E-mail: yanbo.lian@unimelb.edu.au

Animals can perform very complex spatial navigation tasks, but how the brain implements a navigational system to do this is still largely unclear. Recent experimental work discovered egocentric spatial cells that code for the space with respect to the observer, such as egocentric spatial cells in the postrhinal cortex (PoR) [1] and egocentric boundary cells in the retrosplenial cortex (RSC) [2]. The animals use sensory systems, that are egocentric in nature, to explore space, so understanding how egocentric spatial representation of the space arises from sensory input during a learning process is vital to uncover how the brain navigates.

Spatial cells found in rat PoR can be characterized by three aspects: center bearing, center distance, and head direction [1]. Head direction is an allocentric measurement, center bearing is an egocentric measurement that is the angle between the current head direction and the center of the environment, and center bearing is also an egocentric measurement that represents the distance between the animal and the center of the environment. Experimental data shows that PoR cells exhibit diverse spatial properties: some are selective to a preferred head direction, some have a preferred center bearing, some show tuning to center distance, and some have conjunctive encoding of more than one aspect.

In this work, we build a computational learning model based on sparse coding [3] that can learn different types of PoR egocentric spatial cells similar to those observed in real animal brains, using visual information via the superior colliculus [4]. As a virtual rat runs in a simulated environment, the visual input of the virtual rat is captured and then used as the input to train the model. After learning, our model shows different types of egocentric spatial cells that are similar to those found in PoR. This work explains how PoR spatial cells can arise from a learning process with visual input processed by SC, suggesting that the principle of sparse coding might be one of the underlying principles in the brain's navigational system.

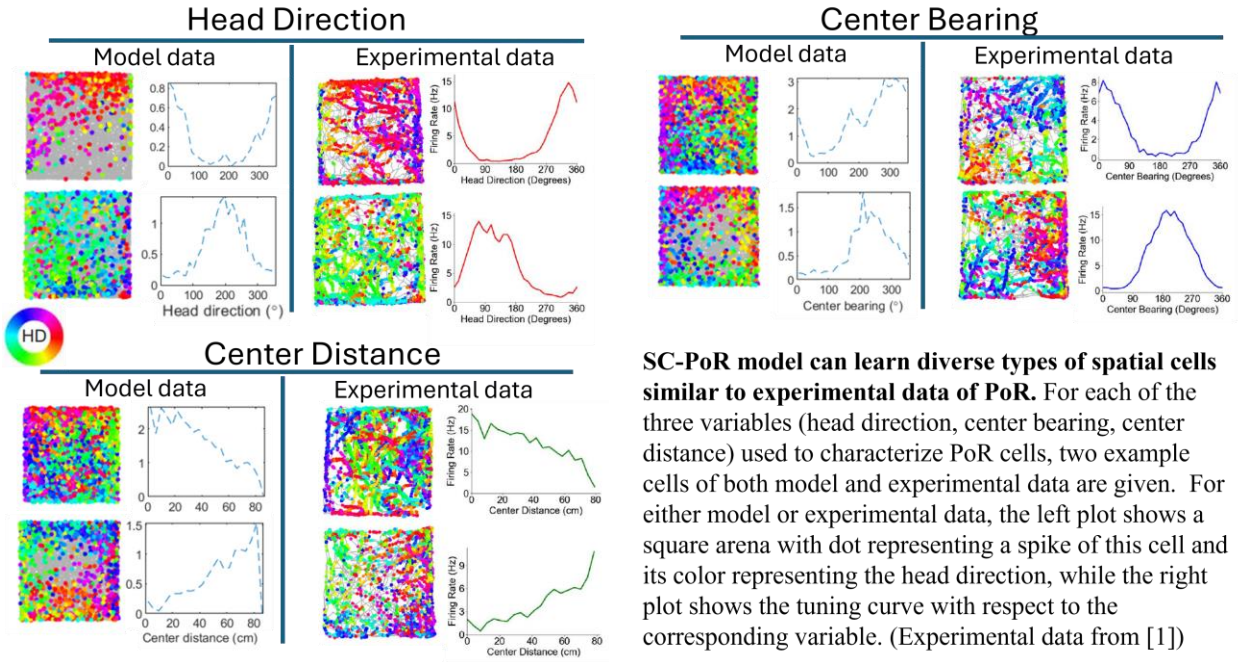

SC-PoR model can learn diverse types of spatial cells similar to experimental data of PoR. For each of the three variables (head direction, center bearing, center distance) used to characterize PoR cells, two example cells of both model and experimental data are given. For either model or experimental data, the left plot shows a square arena with dot representing a spike of this cell and its color representing the head direction, while the right plot shows the tuning curve with respect to the corresponding variable. (Experimental data from [1])

Acknowledgements
This work received funding from the Australian Government, via grant AUSMURIB000001 associated with ONR MURI grant N00014-19-1-2571

References
[1] P. A. LaChance, T. P. Todd, and J. S. Taube, "A sense of space in postrhinal cortex," Science, vol. 365, no. 6449, p. eaax4192, 2019.
[2] A. S. Alexander, L. C. Carstensen, J. R. Hinman, F. Raudies, G. W. Chapman, and M. E. Hasselmo, "Egocentric boundary vector tuning of the retrosplenial cortex," Sci. Adv., vol. 6, no. 8, p. eaaz2322, 2020.
[3] Y. Lian, S. Williams, A. S. Alexander, M. E. Hasselmo, and A. N. Burkitt, "Learning the vector coding of egocentric boundary cells from visual data," J. Neurosci., vol. 43, no. 28, pp. 5180–5190, 2023.
[4] J. M. Brenner, R. Beltramo, C. R. Gerfen, S. Ruediger, and M. Scanziani, "A genetically defined tecto-thalamic pathway drives a system of superior-colliculus-dependent visual cortices," Neuron, 2023.

Stability of Brain Networks in Epilepsy

Jieru Liao[1], Joseph T. Lizier
[1] School of Computer Science and Centre for Complex Systems, University of Sydney, Sydney, Australia
Email: jieru.liao@sydney.edu.au

Epilepsy is a common neurological disorder affecting millions globally[1], often viewed as a brain network disorder characterized by abnormal synchrony or instability. Network neuroscience approaches to epilepsy attempt to characterize how the various components of the underlying network structure are related to various seizure states. These approaches have had success, for example in identifying propagating zones, although they have often focused on functional network analysis, and on measures only indirectly related to network instability. This could be improved by analyzing generative models of the dynamics, and by directly measuring how the network structure relates to instability or lack thereof.

In this study, we employed a one-dimensional Epileptor model from The Virtual Brain platform (TVB) to simulate brain dynamics before and after seizures[2], and then employed the resulting weighted connectivity metrics to model the fluctuations around a stable state. We developed a novel mathematical approach to measure instability of the (linearized) dynamics based on the network structure. This includes introducing a new measure to quantify each node's "driving" and "driven" impact on overall network instability σ^2_{st} (see Fig. a), offering a more direct alternative to characterising instability as compared to traditional graph metrics like node controllability and centrality. To further characterize epileptogenic progression from a structural standpoint, our approach differentiates and explains instabilities caused by focal versus distributed seizures.

By tuning node excitability and coupling parameters, we demonstrate that instability measures differentiate healthy, non-propagating, and propagating seizure states, serving as early warning markers of critical seizure transitions. Moreover, our new mathematics identifies key nodes with strong influence in driving the network away from the stable-state. And crucially, this influence correlates to as their susceptibility to drive seizures as their excitability increases, underlining the potential of this method to identify epileptogenic nodes. Finally, we compared the results to null network models with various aspects of the structure homogenized, which validated the role of network structure in determining the emergence and diffusion of instability. Our method provides a guide for more targeted surgical and neuromodulatory interventions, such as deep brain stimulation and responsive neurostimulation.

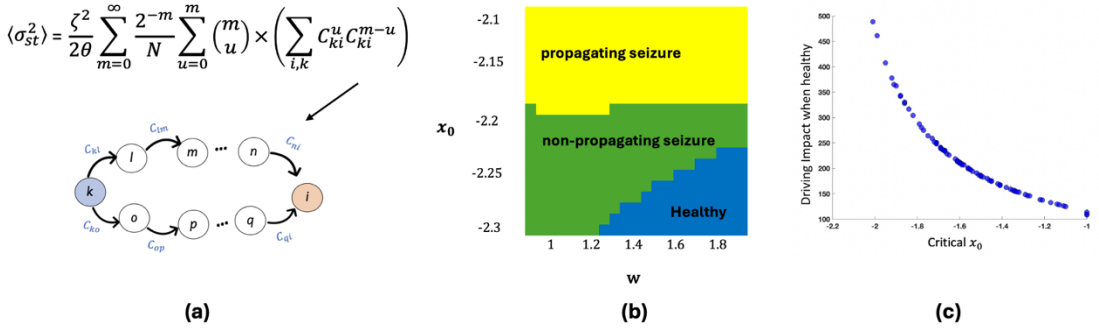

Figure (a) The convergent walks in the network. The impact on stability is represented by the (weighted) count of convergent walks that either originate (driving) or terminate (driven) at the specified node. **(b) Simplified 1D linear analysis** of phase versus TVB parameters x_0 and w corresponds. **(c) Nodes' driving impact** on instability σ^2_{st} provides the ability to quantify node's susceptibility as Epileptic Zone (EZ).

References

[1] Dua, T., De Boer, H. M., Prilipko, L. L., & Saxena, S. (2006). Epilepsy care in the world: results of an ILAE/IBE/WHO global campaign against epilepsy survey. Epilepsia, 47(7), 1225-1231
[2] Proix, T., Bartolomei, F., Guye, M., & Jirsa, V. K. (2017). Individual brain structure and modelling predict seizure propagation. Brain, 140(3), 641-6

Endovascular stimulation of the pudendal nerve

JingYang Liu[1,3], David B Grayden[1,3], Janet R Keast[2], Sam E John[1,3],
[1] Department of Biomedical Engineering, University of Melbourne, Parkville, Australia.
[2] Department of Anatomy and Physiology, University of Melbourne, Parkville, Australia.
[3] Graeme Clark Institute for Biomedical Engineering, University of Melbourne, Parkville, Australia
E-mail: jingyangl4@unimelb.edu.au

Preclinical and clinical studies have identified the pudendal nerve as a promising target for restoring bladder control. Its proximity to accompanying blood vessels in the pudendal canal enables endovascular neurostimulation, a less invasive alternative to conventional implanted electrodes. This study explored the feasibility of excitative stimulation and kilohertz-frequency block of the compound pudendal nerve in sheep using a stent-mounted electrode array. In acute animal experiments, a commercially available hexapolar electrode catheter was introduced into the unilateral internal pudendal artery (Figure 1a) for bipolar stimulation, followed by a custom-made stent-mounted electrode array. Global EMG activity of the pelvic floor muscles was recorded. Both electrode types enabled pudendal nerve stimulation and evoked pelvic floor muscle contractions, with threshold current influenced by electrode-nerve distance and orientation (Figure 1b). Increasing axial inter-electrode distance significantly reduced threshold current. Endovascular kilohertz-frequency nerve conduction block was feasible with the electrode catheter. These findings suggest that endovascular stimulation via a stent-mounted electrode array could be a less invasive alternative to conventional implants for urinary incontinence treatment. Additionally, endovascular pudendal nerve block may offer a solution for bladder-sphincter dyssynergia in spinal cord injury management.

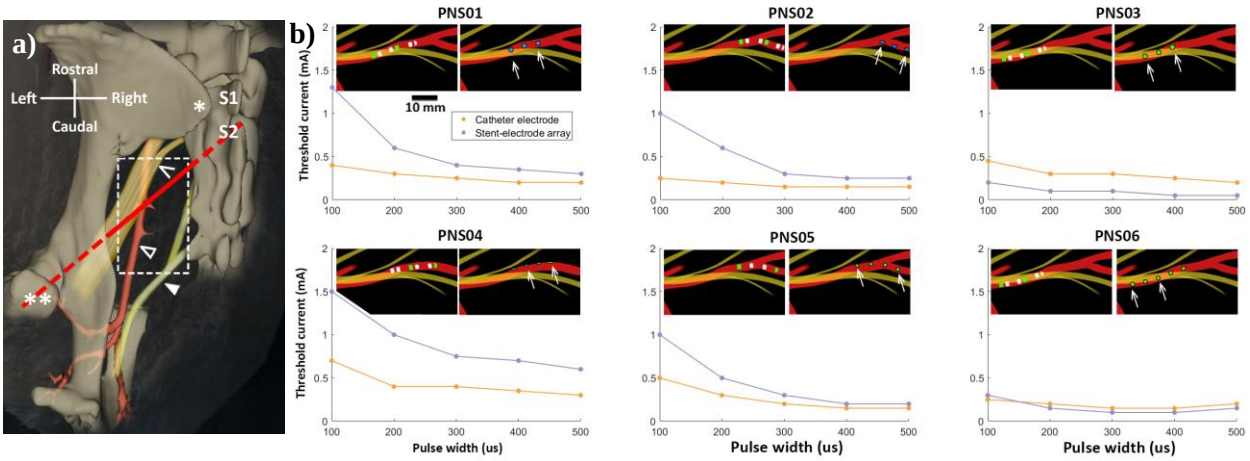

Figure 1. a) Surgical access of the sheep internal pudendal artery through the trans-gluteal approach. Open arrowhead: Sciatic nerve. Unfilled triangle: Internal pudendal artery. Black triangle: The compound pudendal nerve. b) Strength-duration curves of endovascular pudendal stimulation derived from each animal. The inserts are close-ups of where the electrode arrays were implanted near the ischial arch. The left inserts mark the estimated positions of the catheter electrodes, whereas the right inserts mark the stent electrodes. Stent electrodes marked green (PNS3-6) were oriented towards the plane of view (facing dorsally), whereas electrodes marked blue (PNS1 and PNS2) were oriented away from the plane of view (facing ventrally).

Acknowledgements
We acknowledge the expert technical assistance of Mr. Anthony Dornom, Mr. Tom Vale, and Mr. Quan Nguyen. This research was supported by The University of Melbourne's Research Computing Services and the Petascale Campus Initiative. This research was funded by the Australian Government through the National Health and Medical Research Council of Australia (NHMRC) Project Grant 1158912, Development Grant 2000153, US Department of Defence, Epilepsy Research Program CDMRP EP170058 and EP210052.

Epileptic Seizure Prediction using Coherence in Long-Term iEEG and Deep Learning

Sha Lu[1], Lin Liu[1], Jiuyong Li[1], Jordan Chambers[2], Mark J. Cook[2,3], and David B. Grayden[2,3]
[1] STEM, University of South Australia, Adelaide, Australia.
[2] Department of Biomedical Engineering and Graeme Clark Institute, The University of Melbourne, Melbourne, Australia.
[3] Department of Medicine, St. Vincent's Hospital, Melbourne, Australia.
E-mail: Sha.Lu@unisa.edu.au

Epilepsy affects millions of individuals globally, with seizures often lacking effective control and severely impacting quality of life. This study introduces the Coherence-based Seizure Prediction (CoSP) method, which integrates coherence analysis with deep learning to improve seizure prediction and forecasting performance, using long-term intracranial electroencephalography (iEEG) data from the NeuroVista seizure advisory system [1].

As illustrated in Figure 1, the CoSP method first divided iEEG recordings into 10s segments and computed their pairwise channel coherence to capture functional brain connectivity. This coherence matrix was then input to a four-layer convolutional neural network (CNN) to estimate the probabilities of these segments being in the preictal state. The final stage of the framework processed these probabilities to issue seizure warnings.

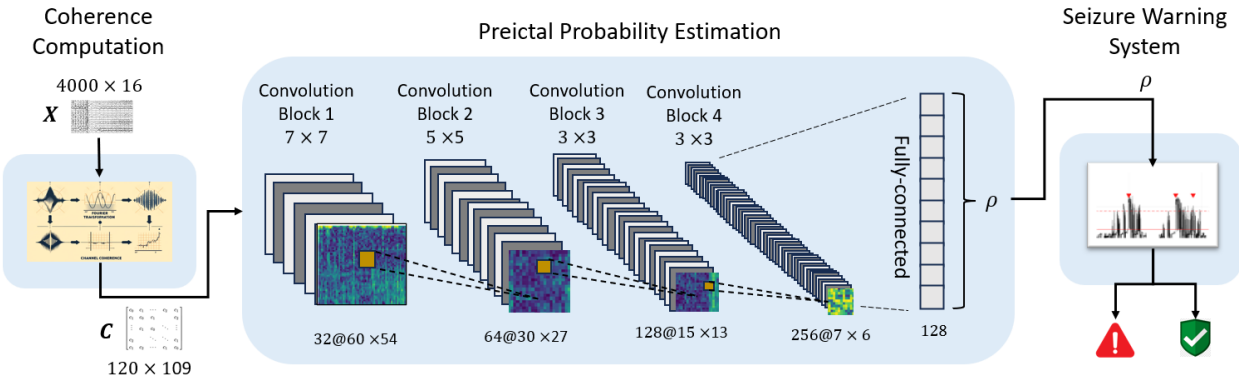

Figure 1. The CoSP method framework comprises three primary modules: (1) coherence computation, which extracts pairwise coherence from 10-second iEEG segments; (2) preictal probability estimation, utilizing a four-layer convolutional neural network (CNN) to estimate the probability of being a preictal state; and (3) a warning system that processes these probabilities to determine and issue seizure warnings.

CoSP was validated on data from 10 patients and demonstrated promising results across preictal intervals ranging from 4 to 180 minutes, albeit with inter-patient variability. Key metrics include seizure sensitivity ranging from 0.63 to 0.92 (median: 0.79), false alarm rates per hour ranging from 0.03 to 0.79 (median: 0.15), and Time in Warning (TiW) ranging from 18% to 35% (median: 27%). Statistically, CoSP significantly outperformed chance predictor (p = 0.001) and demonstrated superiority over most baseline methods using the NeuroVista dataset ($p < 0.05$). These findings highlight the potential of CoSP as an effective tool for seizure prediction, offering improved accuracy, reduced false alarms, and meaningful clinical benefits for patients with drug-resistant epilepsy. CoSP advances the field by leveraging coherence analysis and deep learning to address a critical challenge in epilepsy management.

Acknowledgements
This work was funded by the Australian Government under the Australian Research Council's Training Centre in Cognitive Computing for Medical Technologies (project number ICI70200030).

References

1. Cook, M.J., et al., Prediction of seizure likelihood with a long-term, implanted seizure advisory system in patients with drug-resistant epilepsy: a first-in-man study. The Lancet Neurology, 2013/06/01. 12(6), 563-671.

Long-range cortico-cortical connections shape brain dynamics on rapid timescales

Rishi Maran[1], Eli Muller[1], Ben Fulcher[1],
[1] School of Physics, University of Sydney, Australia.
E-mail: rmar3180@uni.sydney.edu.au

The cerebral cortex takes the form of a sheet of interconnected neurons that interact both through intracortical 'gray-matter' connections along the sheet, and through a complex network of long-range 'white-matter' connections (LRCs) that facilitate rapid communication between distant neural populations. LRCs play a well-established functional role in supporting information processing across distributed neural systems and underpin the prevalent view of the brain as a communication network (or connectome) of functionally specialized regions. However, recent results have challenged this network-based view, showing that key properties of resting-state fMRI dynamics can be accurately captured by simple geometric models that neglect LRCs[1,2]. A key open question thus remains: if LRCs are crucial for cortical function, why do they appear to play a minimal role in capturing key dynamical properties of fMRI?

Here we address this question through a range of investigations using a novel mathematical model of cortical dynamics, in which neural populations interact both through a connectome of specific LRCs and through a sheet of geometrically constrained connections. For a large variety of connectome topologies, we demonstrate that, in spontaneous settings and on long timescales (as per fMRI measurements), simulated brain dynamics increasingly resemble that of a geometric model that excludes the connectome. Our results thus provide a plausible account for the role of LRCs in shaping cortical dynamics on different length and timescales, and explain why LRCs (which predominantly shape fast information processing of precise input stimuli) have a minimal role in shaping brain dynamics on timescales accessible to fMRI.

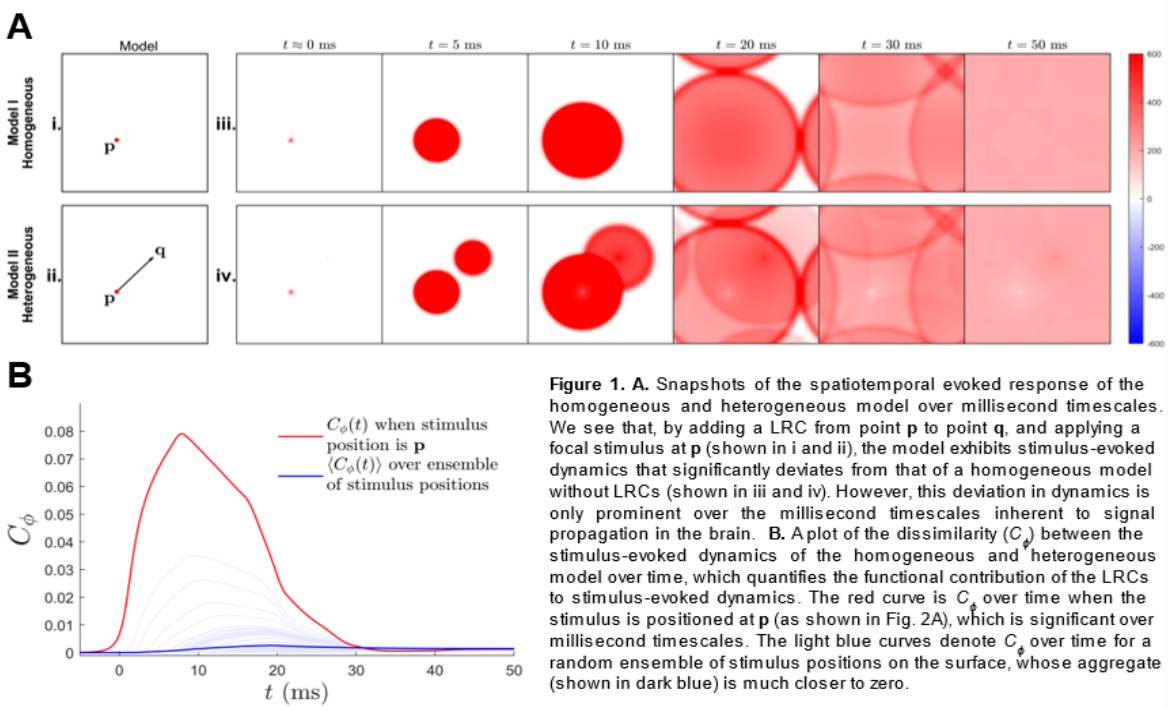

Figure 1. A. Snapshots of the spatiotemporal evoked response of the homogeneous and heterogeneous model over millisecond timescales. We see that, by adding a LRC from point **p** to point **q**, and applying a focal stimulus at **p** (shown in i and ii), the model exhibits stimulus-evoked dynamics that significantly deviates from that of a homogeneous model without LRCs (shown in iii and iv). However, this deviation in dynamics is only prominent over the millisecond timescales inherent to signal propagation in the brain. **B.** A plot of the dissimilarity (C_ϕ) between the stimulus-evoked dynamics of the homogeneous and heterogeneous model over time, which quantifies the functional contribution of the LRCs to stimulus-evoked dynamics. The red curve is C_ϕ over time when the stimulus is positioned at **p** (as shown in Fig. 2A), which is significant over millisecond timescales. The light blue curves denote C_ϕ over time for a random ensemble of stimulus positions on the surface, whose aggregate (shown in dark blue) is much closer to zero.

Acknowledgements
This work was supported by the Australian Government Research Training Program (RTP) Scholarship.

References
1. Gabay, N. C., & Robinson, P. A. (2017). Cortical geometry as a determinant of brain activity eigenmodes: Neural field analysis. Physical Review E, 96(3), 032413.
2. Pang, J. C., Aquino, K. M., Oldehinkel, M., Robinson, P. A., Fulcher, B. D., Breakspear, M., & Fornito, A. (2023). Geometric constraints on human brain function. Nature, 618(7965), 566-574.

Predictive coding and prediction errors in balanced spiking neural networks

Elnaz Nemati[1], Catherine E. Davey[1], Hamish Meffin[1,2], Anthony N. Burkitt[1,2]
[1] Department of Biomedical Engineering, The University of Melbourne, Victoria, Australia.
[2] Graeme Clark Institute, The University of Melbourne, Victoria, Australia.
E-mail: fnemati@student.unimelb.edu.au

Predictive coding theory suggests that the brain processes sensory information efficiently by integrating feedforward and feedback pathways to minimize prediction errors [1]. Sensory inputs detected in Layer 4 are compared with predictions in Layer 2/3, with discrepancies (prediction errors) relayed to deeper cortical layers (5/6) and higher brain regions to refine future predictions [2]. When inputs match predictions, excitation and inhibition remain balanced, but mismatches cause selective neuronal activation, with prediction error neurons firing only when inputs deviate significantly.

Our research extends Denève's model [3], where each population of neurons functions as a decoder, allowing inhibitory neuron estimations to track excitatory neuron estimations closely. This configuration ensures the membrane potential accurately reflects prediction errors, resulting in a sparsely balanced network. The novelty of our approach lies in demonstrating that sparsity and selectivity in neuronal firing naturally emerge from these mechanisms of estimation and balance by setting the synaptic weights as Gabor filters, which reflect the receptive field profiles of neurons in the primary visual cortex (V1). We test this model using visual stimuli to investigate its biological relevance. Additionally, we explore these dynamics within a hierarchical spiking neural model representing Layer 4 and Layer 2/3 of V1, an aspect of predictive coding that has not been thoroughly studied in the context of spiking neural models. The model for Layer 2/3 consists of two excitatory populations encoding prediction errors. Positive error neurons fire when a feature is detected in the sensory input but absent in the feedback (sensory-driven mismatches), while negative error neurons fire when a feature is predicted but missing from the sensory input (prediction-driven mismatches). These excitatory populations are balanced by three inhibitory populations designed to maintain a dynamic balance of activity. The circuit design is inspired by biological connectivity and the Hertäg prediction error circuit [4], though it is simplified with fewer populations and connections. Somatostatin (SOM) inhibitory neurons suppress the distal dendrites of pyramidal neurons, activating only during mismatches between feedforward (sensory-driven) and feedback (prediction-driven) inputs. Parvalbumin (PV) inhibitory neurons regulate excitatory populations through two subtypes: PV1 neurons, driven by feedback (prediction) signals, maintain balance by inhibiting positive error neurons, while PV2 neurons, driven by feedforward (sensory) signals, maintain balance by inhibiting negative error neurons.

We implemented the hierarchical spiking neural network using leaky integrate-and-fire neurons in Brian2. Layer 4 consists of 4096 excitatory and 1024 inhibitory neurons, while layer 2/3 includes 1024 positive error neurons, 1024 negative error neurons, and three inhibitory populations comprising 64 PV1, 64 PV2, and 64 SOM neurons. Synaptic weights are designed using Gabor filters with six orientations and four phases. The inputs are fixed gratings, and feedback is tested under matched and unmatched conditions. Synaptic scaling follows Denève's framework [3], where synaptic weights are normalized by their respective norms, ensuring stable, size-independent network dynamics and preserving the balance between excitation and inhibition as the network scales.

Our analysis using grating stimuli reveals a tightly balanced interaction between excitatory and inhibitory input signals, especially during feature matches. The results show that SOM neurons ensure the distal compartments of pyramidal neurons activate only when there is a mismatch between feedforward (sensory-driven) and feedback (prediction-driven) inputs. PV1 neurons suppress positive error excitatory neurons whose Gabor profiles match the feedback input, preventing unnecessary firing. Neurons with profiles present in the feedforward input but absent in the feedback remain uninhibited and can fire, signalling sensory-driven mismatches. Neurons with matching Gabor profiles in both feedforward and feedback inputs maintain balance and rarely spike, preserving circuit stability. PV2 neurons suppress negative error neurons with Gabor profiles matching the feedforward input. Neurons with profiles that matching the feedback but differ from the feedforward input are uninhibited, encoding negative prediction-driven mismatches. These activity patterns are consistent with experimental findings from Jordan et al. [5]. By examining feedback mechanisms, we investigate the broader influence of stimuli on neural circuits, offering deeper insights into the visual cortex's roles in end-stopping effects. This study contributes to a better understanding of visual processing and its applications in enhancing artificial vision systems, highlighting predictive coding as a promising alternative to backpropagation for neuromorphic integration.

References

1. Rao, R. P. N. & Ballard, D. H. (1999) Nature Neuroscience, 2(1): 79-87.
2. Bastos, A. M. et. al (2012) Neuron, 76(4): 695-711.
3. Denève, S., & Machens, C.K. (2016) Nature Neuroscience, 19(3):375-382.
4. Hertäg, L., & Clopath, C. (2022) Proc. Natl. Acad. Sci., 119(13): e2115699119 (pp.1-12).
5. Jordan, R., Keller, G. B., & Kriegeskorte, N. (2020) Neuron, 108(6): 1194-1206.

Neuronal Transfer Entropy: a Biophysical Model of Information Flow Based on Dynamic Causal Modelling

Leonardo Novelli[1] and Adeel Razi[1,2,3]
[1]School of Psychological Sciences and Monash Biomedical Imaging, Monash University, Australia.
[2]Wellcome Centre for Human Neuroimaging, University College London, United Kingdom.
[3]CIFAR Azrieli Global Scholars Program, Toronto, Canada.
E-mail: leonardo.novelli@monash.edu

Transfer entropy[1] and Dynamic Causal Modelling (DCM) [2] are popular methods for inferring brain connectivity from neuroimaging time series. Here, we combine their strengths by mathematically deriving Transfer Entropy under the spectral DCM[3] model for resting-state fMRI. This approach leverages Transfer Entropy's ability to quantify information flow and DCM's ability to infer neuronal interactions from indirect neuroimaging measurements.

The main idea is illustrated in Fig. 1. First, we use DCM to fit a model to the observed data and infer the requisite parameters, including the effective connectivity matrix that describes the directed excitatory or inhibitory effects between brain regions. Then, we use these parameters to derive a DCM-based parametric estimator of Transfer Entropy, i.e., the amount of information (in bits) transferred between brain regions. The mathematical derivations are based on the theory of stochastic processes and spectral factorisation[4,5]. We derived the Neuronal Transfer Entropy analytically in a toy system and are working on numerical approximations to enable applications to real data at scale.

This novel approach renders Neuronal Transfer Entropy robust to measurement noise[6] and other confounding factors, e.g. the hemodynamic response in fMRI. It also quantifies the uncertainty of the Neuronal Transfer Entropy estimates via Bayesian inference. In conclusion, Neuronal Transfer Entropy is a mechanistic, neuro-physiologically grounded model of information transfer that links synaptic physiology to information processing—in a formal and empirically testable fashion. It allows us to precisely measure when, where, and how much information flows in the brain.

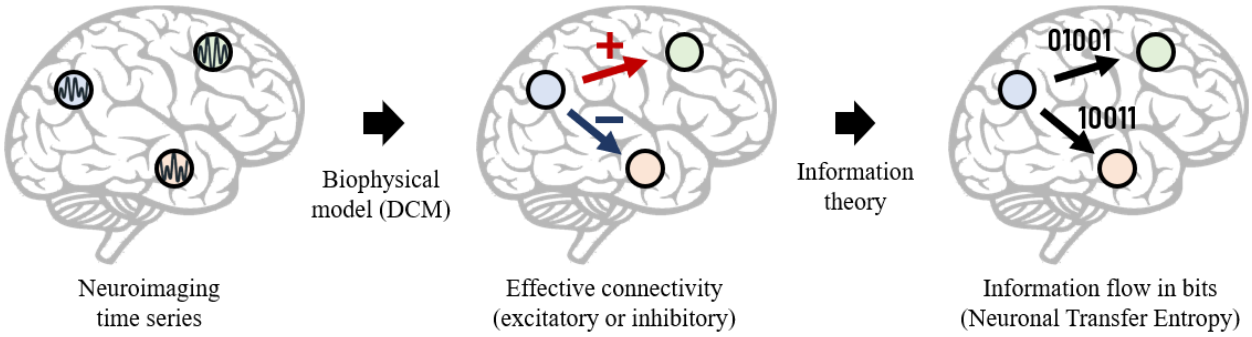

Figure 1. Neuronal Transfer Entropy quantifies information flow using brain connectivity inferred via biophysical models. This solves current issues in estimating the information flow directly from the neuroimaging time series.

References

1. Schreiber, T. (2000). Measuring Information Transfer. Physical Review Letters, 85(2), 461–464.
2. Friston, K. J., Harrison, L., & Penny, W. (2003). Dynamic causal modelling. NeuroImage, 19(4), 1273–1302.
3. Razi, A., & Friston, K. J. (2016). The Connected Brain: Causality, models, and intrinsic dynamics. IEEE Signal Processing Magazine, 33(3), 14–35.
4. Barnett, L., & Seth, A. K. (2017). Detectability of Granger causality for subsampled continuous-time neurophysiological processes. Journal of Neuroscience Methods, 275, 93–121.
5. Kucera, V. (1991). Factorization of rational spectral matrices: A survey of methods. International Conference on Control 1991. Control '91, 2, 1074–1078.
6. Friston, K. J., Bastos, A. M., Oswal, A., van Wijk, B., Richter, C., & Litvak, V. (2014). Granger causality revisited. NeuroImage, 101, 796–808.

Computational Fluid Dynamics Modelling of Blood Flow in Venous Stents and Endovascular Neural Interfaces

Weijie Qi[1,2], Andrew Ooi[3], David B. Grayden[1,2], and Sam E. John[1,2]
[1] Department of Biomedical Engineering, The University of Melbourne, Parkville, Australia
[2] Graeme Clark Institute for Biomedical Engineering, The University of Melbourne, Parkville, Australia
[3] Department of Mechanical Engineering, The University of Melbourne, Parkville, Australia
E-mail: james.qi@unimelb.edu.au

With growing interest in endovascular stents as neural interfaces, this study evaluates the impact of stent-electrode arrays on blood flow and tissue response following implantation in sheep veins. Computational Fluid Dynamics (CFD) modeling was used to simulate blood flow in stented vessel segments (n = 8), which were reconstructed and validated using venography and micro-CT scans. Doppler ultrasound measurements provided venous flow boundary conditions and validated blood flow dynamics. By analyzing vessel lumen size and blood flow changes over one month, the study identifies key factors influencing venous flow and vascular remodeling. Findings indicate that venous flow—particularly Wall Shear Stress (WSS) immediately post-implantation—correlates with tissue response patterns over time. This work addresses gaps in cerebral venous stenting and endovascular neural interfaces, providing insights for improved risk assessment and design strategies to minimize blood flow disruptions and device-related complications.

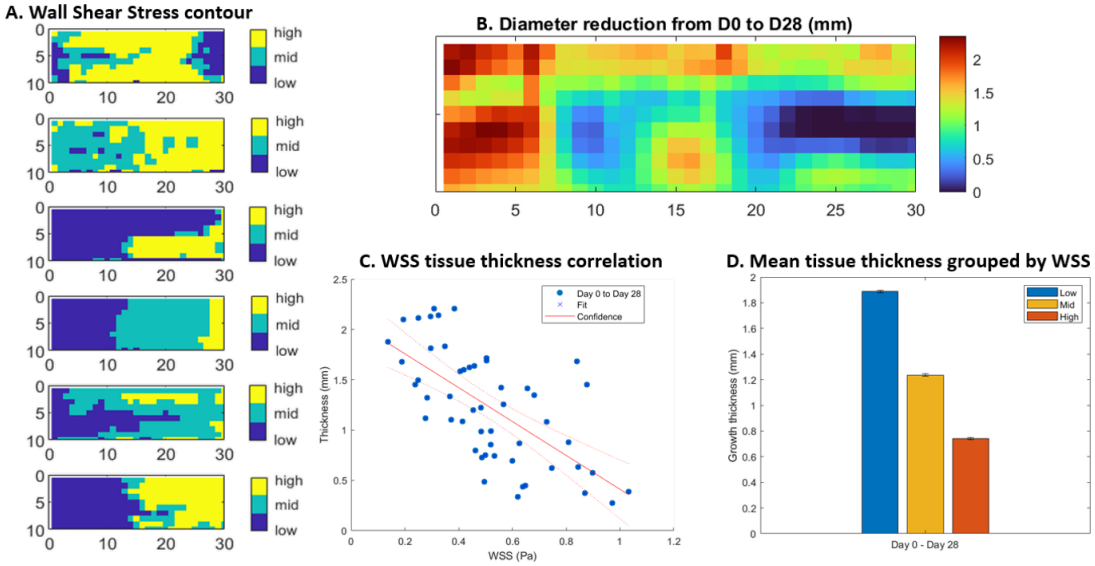

Figure 1. Wall Shear Stress (WSS) and tissue growth patterns in sheep after 1 month of stent implantation. **A:** WSS contour maps across different time points (from top to bottom: Day 0 – before implantation, Day 0 – just after implantation, Day 7, Day 14, Day 21, and Day 28), with the blood vessel lumen wall divided into low, mid, and high WSS regions. Blood flow direction is from left to right. **B:** Diameter reduction along the stented region of the target blood vessel over 1 month, indicating greater tissue growth at the stent inlet. **C:** Correlation between WSS at Day 0 – just after implantation and tissue growth thickness over 4 weeks ($R = -0.6544$; $P < 0.05$), demonstrating an inverse relationship. **D:** Mean tissue growth over 1 month categorized by low, mid, and high WSS regions from Day 0 – just after implantation.

Acknowledgements
The research was supported by research grants from the USA Department of Defense Office of the Congressionally Directed Medical Research Programs (CDMRP), EP170058 and National Health and Medical Research Council of Australia (NHMRC) grant 1158912. Weijie Qi is funded by the China Scholarship Council (CSC) from the Ministry of Education of P.R. China, CSC NO. 202008240002. The CFD modelling was supported by The University of Melbourne Research Computing Services and the Petascale Campus Initiative. The authors would like to thank Huakun Xin for his assistance with the design of the stent used in the study.

BRAIN-WIDE CALCIUM IMAGING IN ZEBRAFISH AND NETWORK ANALYSIS REVEAL CELL-LEVEL FUNCTIONAL NETWORK PROPERTIES OF SEIZURE SUSCEPTIBILITY

Wei Qin[1], Jessica Beevis[2], Maya Wilde[2], Sarah Stednitz[1], Josh Arnold[2], Itia Favre-Bulle[2], Ellen Hoffman[3], Ethan K. Scott[1]
[1] Department of Anatomy and Physiology, University of Melbourne, VIC, Australia
[2] Queensland Brain Institute, University of Queensland, QLD, Australia
[3] Department of Neuroscience, Yale School of Medicine, Yale University, New Haven, CT, USA
E-mail: wei.qin@unimelb.edu.au

Epilepsy is a neurological disorder that causes recurrent seizures, but the underneath mechanisms are still unclear. Traditional methods, using data from humans, nonhuman primates, or rodents, have limitations in resolving the activity of single cells. An approach that captures the dynamics of individual neurons and their interactions within brain-wide networks could therefore be of great utility in understanding epilepsy. Calcium imaging offers such an approach, as they allow for simultaneous in-vivo recording of neuronal activity across the brain at cellular resolution [1]. Zebrafish, sharing genetic and physiological similarities with humans, can exhibit seizure-like behaviors due to drugs like Pentylenetetrazol (PTZ), which blocks inhibitory GABAergic signaling. Mutations in the scn1lab gene, encoding a sodium channel, can also cause spontaneous seizures [2, 3]. We utilised network analyses and computational modelling to statistically quantify differences in functional network topology and dynamics between wildtype and scn1lab mutant zebrafish larvae under baseline and post-PTZ condition, as observed through calcium imaging. Specifically, we examined the functional network of active neuronal cells involved in ictogenesis across microscopic to macroscopic scales. Our study reveals significant and consistent changes in brain network connectivity, indicating that scn1lab mutations impact brain structure and functions. Additionally, we employed generative network modelling [4] (GNM, Eq. 1) using similarities between ROIs as the wiring rewards (K_{ij}) to investigate the impact of scn1lab mutations and PTZ on brain network formation. The wiring rules, implemented via an edge-addition algorithm, consider Euclidean distances (D_{ij}) between ROIs as the cost factor [4]. Simulations for both WT and scn1lab mutants adhere to the same network growth principles but differ in their scaling parameters, η and γ (Figure A). Kolmogorov-Smirnov (KS) energy similarity was utilized for evaluating simulation performance [4]. Partial least squares-discriminant analysis (PLS-DA) was applied to classify models of each region to best describe a genotype [5] (Figure B). Results from both pre-PTZ and overall stages highlight brain regions (Figure C) responsible for key traits of scn1lab$^{-/-}$ animals, particularly implicating the pallium and habenula (Figure D), whose baseline properties significantly differ from WT and strongly correlate with the animals' genotypes. Such predictive models would facilitate hypothesis-driven tests of brain function through targeted ablations or optogenetic manipulations in future studies.

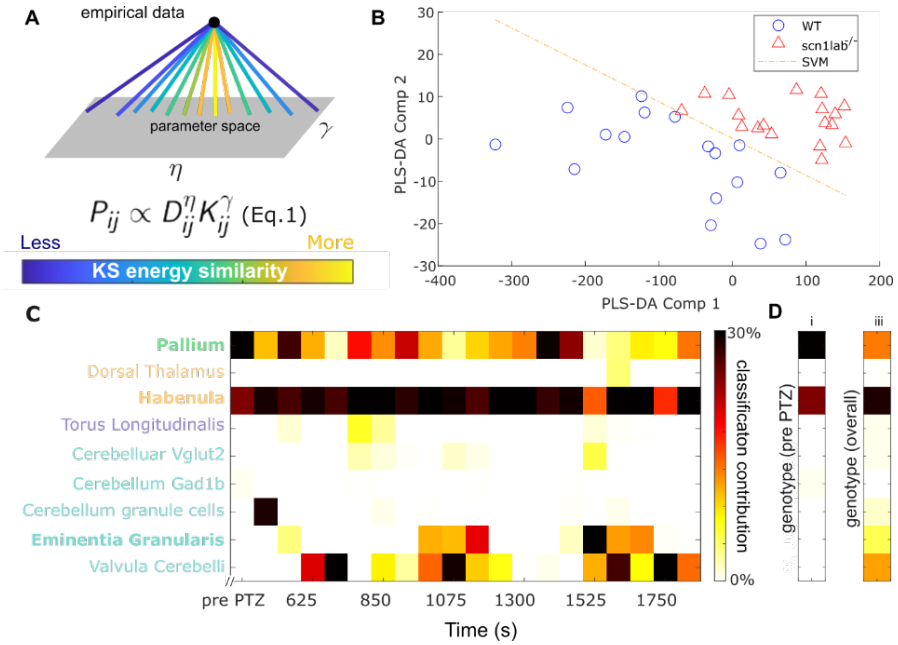

Figure A. Generative network modelling (GNM) simulates wiring principles, evaluated by KS similarity. **B.** The model accurately classifies and predicts genotypes without relying on phenotypes. **C.** It assesses the contribution of each region to correct classification at each PTZ stage. **D.** The pallium and habenula are identified as the main contributors to the classification.

Acknowledgements
The authors would like to thank the UQBR aquatics team for maintenance of fish stocks. This project is supported by NHMRC, ARC, Simons Foundation and NIH (US).

References

1. Kettunen, P. (2012). **Calcium Imaging in the Zebrafish**. In: Islam, M. (eds) Calcium Signaling. Advances in Experimental Medicine and Biology, vol 740. Springer, Dordrecht.
2. Afrikanova T, et al. (2013) **Validation of the Zebrafish Pentylenetetrazol Seizure Model: Locomotor versus Electrographic Responses to Antiepileptic Drugs**. PLoS ONE 8(1): e54166.
3. Paige A Whyte-Fagundes, et al. (2024), **Testing of putative antiseizure medications in a preclinical Dravet syndrome zebrafish model**, Brain Communications, Volume 6, Issue 3
4. Hills TT. (2024) **Generative Network Models and Network Evolution.** In: Behavioral Network Science: Language, Mind, and Society. Cambridge University Press; 2024:46-60.
5. Barker M, Rayens W (2003). **Partial least squares for discrimination**. J Chemometrics. 2003; 17(3):166–73.

Predicting Eye Movement Intentions from Brain Signals

Suleman Rasheed[1,3], James Bennett[2], Peter Yoo[2], Anthony N. Burkitt[1,3], David B. Grayden[1,3],
[1] Department of Biomedical Engineering, The University of Melbourne,
[2] Synchron Inc, Brooklyn, NY,
[3] Graeme Clark Institute, The University of Melbourne.
E-mail: sulemanr@student.unimelb.edu.au

Objective: Eye tracking is a widely used assistive technology for individuals with physical disabilities but is ineffective for those lacking voluntary eye control, such as completely locked-in patients. An alternative approach is decoding brain signals related to saccade planning, forming an Oculomotor Brain-Computer Interface (BCI) [1]. Previous oculomotor BCI studies have relied on invasive microelectrode implants in non-human primates, which carry surgical risks, while non-invasive EEG studies in humans have used electrooculogram (EOG) artifacts, which reflects eye muscle activity rather than directly capturing neural correlates of saccade planning. This study investigates an alternative approach using an oculomotor BCI based on brain signals recorded from a minimally invasive endovascular Stentrode™ device [2] implanted in the supplementary motor area of a patient with Amyotrophic Lateral Sclerosis (ALS).

Approach: The patient performed visually-guided and free-viewing saccade tasks in four directions (left, right, up, down), while simultaneously recording eye gaze and neural activity.

Main Results: Evoked responses revealed *Saccadic ERPs* (Event-Related Potentials), which appear prior to saccade onset and peak shortly after saccade execution (Figure 1). Notably, for free-viewing saccades, these ERPs were consistent across directions, suggesting a neural signal independent of target location. Classification of saccade versus rest trials achieved a mean AUC-ROC of 0.84 within-session and 0.80 cross-session. Furthermore, as shown in Figure 2, pre-saccade classification yielded results comparable to decoding post-saccade or combined pre+post-saccade trials, demonstrating reliable detection of saccadic intention. The prediction of saccade direction reached an AUC-ROC of 0.75 for the best binary contrasts (left vs. up and left vs. down).

Significance: This proof-of-concept study demonstrates the feasibility of an oculomotor BCI in an ALS patient with a minimally invasive endovascular device. These findings provide a foundation for further research on oculomotor BCIs in human subjects and highlight their potential for assistive applications, either as standalone BCIs or integrated into multimodal systems.

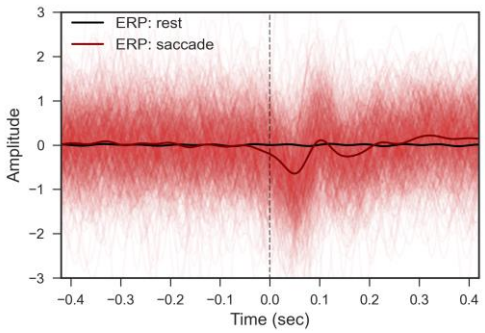

Figure 1. Individual saccade trials (N=606) and evoked responses for rest and saccade trials from independent component IC7, time-locked to saccade onset during free-viewing saccades.

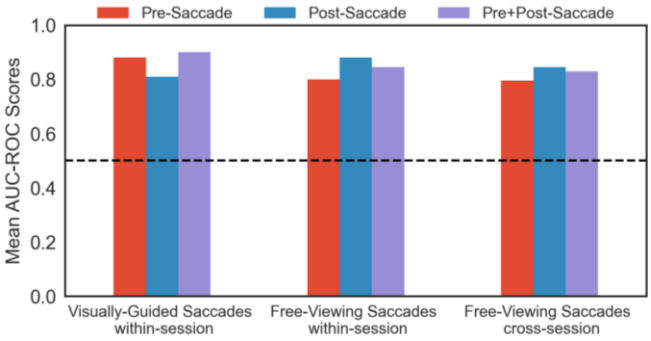

Figure 2. Comparison of saccade onset prediction across three intervals: pre-saccade [-500, 0] ms, post-saccade [0, 500] ms, and pre+post-saccade [-250, 250] ms.

Acknowledgements
This work was funded by the Australian Government under the Australian Research Council's Training Centre in Cognitive Computing for Medical Technologies (project number ICI70200030).

References

[1] N. Jia *et al.*, "Decoding of intended saccade direction in an oculomotor brain-computer interface," *J. Neural Eng.*, vol. 14, no. 4, 2017.
[2] P. Mitchell *et al.*, "Assessment of Safety of a Fully Implanted Endovascular Brain-Computer Interface for Severe Paralysis in 4 Patients," *JAMA Neurol.*, vol. 80, no. 3, p. 270, Mar. 2023.

Modelling the temperature profile of the retina in response to optical stimulation

Daniel B Richardson[1], James Begeng[1], Paul R Stoddart[1], Tatiana Kameneva[1,2]
[1] Department of Engineering Technologies, School of Engineering, Swinburne University of Technology, Australia
[2]Iverson Health Innovation Institute, Swinburne University of Technology, Australia
Email: danbrich7@gmail.com

Electrical stimulation of neurons has been used as a reliable technique to elicit action potentials in implantable devices. Through external forms of generating neuronal response, people with photoreceptor damage from diseases such as retinitis pigmentosa, can retain some form of vision through electrical stimulation of healthy retinal ganglion cells. Recently, novel optical stimulation techniques have been developed as alternatives to electrical stimulation. One approach involves applying near infrared wavelengths of light to the neuron, which generates a neural impulse in response. Optical stimulation may increase the resultant visual acuity compared to electrical stimulation as it does not apply any current and thus has no current spread. As a result of applying light stimulation, the retina experiences an increase in temperature. For this reason, modelling the temperature profile within the retina is vital in testing the feasibility of optical stimulation techniques.

To model the temperature profile in a retina environment that experiences optical stimulation, a Monte Carlo simulation was implemented in MATLAB. The environment consisted of four layers; a 100µm layer of water, a 4µm layer of gold nanorods with 10% surface coverage, 350µm of retinal tissue, and a 100µm layer of glass, with a total model size of 350x350x450µm. A 950nm wavelength pencil beam was used to simulate near infrared stimulation at an angle perpendicular to the x-y plane, at varying powers that matched the experimental values of Begeng et al (2023), 6.6kW/cm^2 and 8.8kW/cm^2. Two procedures were run at different stimulation durations, 100µs and 500µs. A temperature sensor was placed in the model 15µm above the gold nanorod surface, to mimic the experimental procedure. Each layer had specified coefficients obtained from literature, which included the absorption coefficient (μ_a), scattering coefficient (μ_S), scattering anisotropy, volumetric heat capacity, and thermal conductivity. The simulation models the temperature profile through finite element modelling of the defined geometry, dividing the model into small voxels and analysing the temperature profile of each time point. It determines the temperature through tracking the photon paths of the stimulation beam, monitoring how it progresses through the tissues via their varying scattering coefficients and refractive indexes. It then models the florescence and absorption of the tissues through probabilistic determination. The amount of photons absorbed, and its associated power, is then used in conjunction with the heat equation to determine the temperature.

The simulation model demonstrated general agreement with the experimental results, showing comparable peak temperatures and maintaining a consistent trend with the varying pulse durations. Furthermore, the proposed model allows for estimation of the temperature profile on the retinal surface, which is difficult to measure experimentally.

Whilst the model does understate the time taken for the retinal tissue to cool down after the stimulation pulse, compared to the experimental values, this can be addressed via increasing the complexity of the model. Future work may also include defining temperature- and wavelength-dependent medium coefficients, the implementation of convection cooling processes, and using an active neuronal tissue, such as Hodgkin-Huxley type models.

References

JM Begeng, W Tong, B Rosal, M Ibbotson, T Kameneva, PR Stoddart, Activity of retinal neurons can be modulated by tunable near-infrared nanoparticle sensors, ACS Nano 17 (3), 2079 – 2088, 2023.

Learning the spatial and temporal properties of neurons in primary visual cortex using a spike-based network with video stimuli

Marko A. Ruslim[1], Martin J. Spencer[1], Hamish Meffin[1], Yanbo Lian[1], Anthony N. Burkitt[1,2]
[1] Department of Biomedical Engineering, University of Melbourne, Australia
[2] Graeme Clarke Institute, University of Melbourne, Australia.
E-mail: mruslim@student.unimelb.edu.au

The emergence of visual cell properties in the brain can be explained by computational models such as sparse coding [1]. Most models, however, employ rate-based dynamics and learning, and use static image stimuli. Since visual sensory experience is dynamic, using spatio-temporal video stimuli more accurately reflects biological vision processing. In this study, we build upon our previous biologically realistic spiking network [2], incorporating spatio-temporal processing [3], to investigate how different spike-timing-dependent plasticity (STDP) rules and video speeds influence receptive field (RF) formation. The model processes natural video stimuli through a biologically inspired hierarchy: input from natural video is first processed by lateral geniculate nucleus (LGN) neurons with spatio-temporal properties before being learned by primary visual cortex (V1) neurons through STDP.

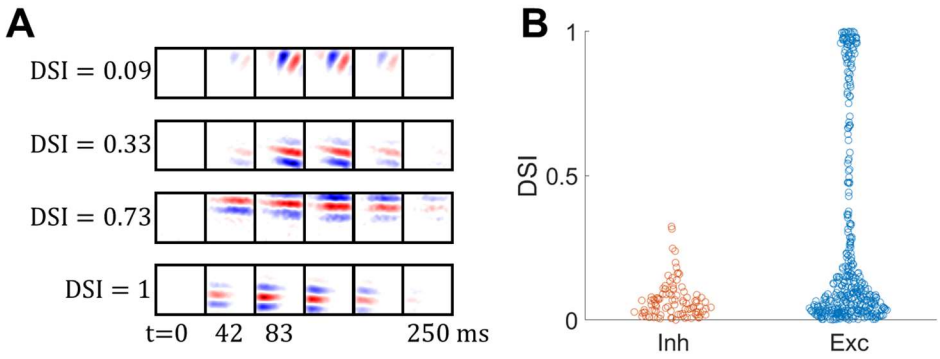

Figure 1. (A) Spatio-temporal RFs of four chosen excitatory neurons. Each row represents one RF, each box is a snapshot of the spatial RF. The direction-selectivity index (DSI) is annotated. (B) Distribution of DSI for excitatory and inhibitory neurons. Each circle is a DSI of a neuron, with jitter in the x-axis corresponding to the density of points.

Among different variants of STDP used in this study, triplet STDP [4] was shown to be more robust to video speeds compared to asymmetrical STDP and symmetrical STDP. RFs formed with triplet STDP were well described by Gabor filters, with a higher proportion of oriented RFs. In contrast, symmetrical STDP produced a greater proportion of non-oriented RFs. These findings suggest that the brain may employ an STDP rule similar to the triplet model. Video speed also affects the diversity of RF shapes: static images led to more uniform RF shapes, while video increased shape diversity, ranging from blob-like to oriented Gabor-like RFs. This may be due to the temporal information in video, such as motion, which is absent in static stimuli. Lastly, when incorporating both spatial and temporal properties in the input LGN neurons, the output V1 neurons were able to learn diverse spatio-temporal properties, such as direction selectivity. The model distributions of excitatory and inhibitory direction-selective index (see Figure 1) resemble the distributions found from experimental recordings.

Acknowledgements
This work was supported by the Australian Government Research Training Program Scholarship.

References
1. Olshausen, B.A. and Field, D.J.: **Emergence of simple-cell receptive field properties by learning a sparse code for natural images.** *Nature* 1996, 381(6583), 607–609.
2. Ruslim, M.A. *et al.*: **Emergence of Sparse Coding, Balance and Decorrelation from a Biologically-Grounded Spiking Neural Network Model of Learning in the Primary Visual Cortex**. *bioRxiv*. 2024.
3. Ruslim, M.A., Lian, Y. and Burkitt, A.N.: **Learning spatio-temporal V1 cells from diverse LGN inputs**. *bioRxiv*. 2023.
4. Pfister, J.P. and Gerstner, W.: **Triplets of spikes in a model of spike timing-dependent plasticity**. *J. Neurosci*. 2006, 26(38), 9673–9682.

Using natural images to compute receptive fields in primary visual cortex

Manula A. Somaratna[1], **Alan W. Freeman**[1]

[1] Save Sight Institute, University of Sydney, Sydney, Australia.
E-mail: manula.somaratna@sydney.edu.au

Introduction. The receptive field of a visual neuron conveys valuable information about the cell's signalling properties – visual field location, spatiotemporal characteristics, and more. A variety of stimuli have been used to compute the receptive field, including spots, bars, gratings, and white noise. We instead aimed to use stimuli, natural images, which neurons have evolved and developed to process. **Methods.** Stimuli were photographs of macaque monkeys [1] and were presented to a signal-processing model of the macaque visual system [2, 3]. The model included cones, horizontal cells, bipolar cells, ganglion cells, geniculate cells, and both excitatory and inhibitory cells in layer 4Cβ of primary visual cortex. Each cell was implemented as a first-order differential equation, and all equations were solved simultaneously to obtain time-varying responses. Receptive fields were calculated by presenting each image for 50 ms, weighting the image by the cell's peak response, adding all weighted images, and normalising the sum by the number of images (about 1600). As a control we also used gratings which varied across the full range of orientations, spatial frequency, and spatial phase. Receptive fields were calculated from responses to pulsed gratings using the same stimulus/response correlation method as for natural images. **Results.** The receptive field obtained with images approached that for gratings as the number of images increase. For the cell shown in the figure, the correlation coefficient between the two receptive field types asymptoted to 0.74 ($p < 0.001$). This is quite representative of the coefficient, 0.69, for all 529 neurons in our sample. **Discussion.** While neurons in primary visual cortex respond well to gratings, the preferred stimulus for downstream cells is typically unknown. Finding optimal stimuli for these downstream cells may be assisted by calculating their receptive fields from responses to natural images.

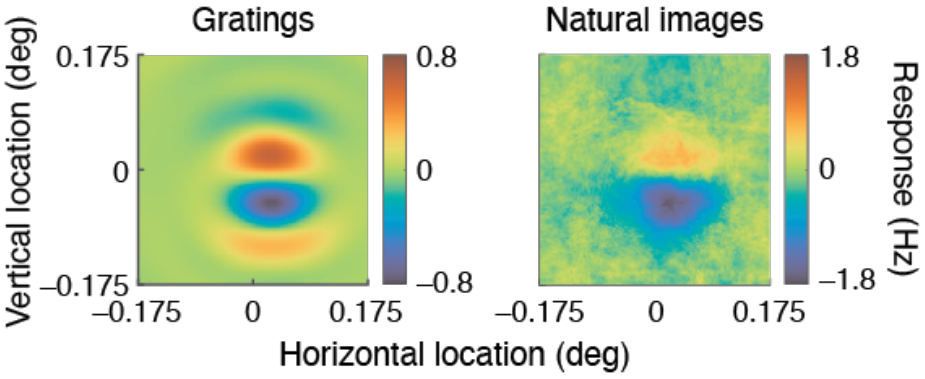

Figure 1. The upstream visual system of a macaque monkey was simulated with a signal-processing model. The figure shows the receptive field of an excitatory neuron in the input layer of primary visual cortex. The receptive field was calculated from the responses of both pulsed gratings (left) and natural images (right). Blue and red indicate areas in which light decreased and increased impulse rate, respectively.

References

1. Deng, J., Dong, W., Socher, R., Li, L.-J., Li, K., and Fei-Fei, L. **ImageNet: A large-scale hierarchical image database.** Paper presented at the *IEEE Conference on Computer Vision and Pattern Recognition*, 2009.
2. Somaratna, M. A. and Freeman, A. W. **Using natural images to compute receptive fields in primary visual cortex.** Paper presented at the annual scientific meeting of the *Society for Neuroscience,* Washington, D.C, 2024.
3. Somaratna, M. A. and Freeman, A.W. **The receptive field construction of midget ganglion cells in primate retina.** *Journal of Neurophysiology* 2025, 133: 268-285. doi:10.1152/jn.00302.2024.

Temporal Sparseness in the Response of Leaky Integrate-and-Fire Neurons

Martin J Spencer[1], Marko Ruslim[1], Yanbo Lian[1], Hinze Hogendoorn[2], Hamish Meffin[1] Anthony N, Burkitt[1,3],
[1] Biomedical Engineering, University of Melbourne, Parkville, Australia.
[2] School of Psychology and Counselling, Queensland University of Technology, Brisbane, Australia.
[3] Graeme Clark Institute, University of Melbourne, 3053 Carlton, Australia
E-mail: martin.spencer@unimelb.edu.au

Biological spiking neural networks (SNNs) and artificial neural networks (ANNs) are known to benefit from the use of sparse coding [1]. In this energy efficient approach, each neuron responds strongly only to a specific feature present in a minority of inputs.

To find the SNN model parameters that lead to sparse coding the response sparseness of a single Leaky Integrate-and-Fire (LIF) neuron with an adaptive spike threshold and without synaptic learning rules was used. Informed by these results a recurrently connected network of these neurons equipped with spike-timing dependent plasticity rules was used to learn sparse visual features in a set of natural images.

In both models it was observed that a sparse response was not purely an outcome of the correct choice of synaptic learning rules. A sparse code additionally required a specific set of input encoding and model neuron dynamics (**Figure 1**). Specifically, in the single neuron model it was found that the total spikes per second input to each LIF neuron must be sufficiently high, the neurons must have a sufficiently high threshold (i.e., generate a low output spike rate) and sufficiently short duration (i.e., fast) membrane time constant. Similar observations were made in the recurrent network model.

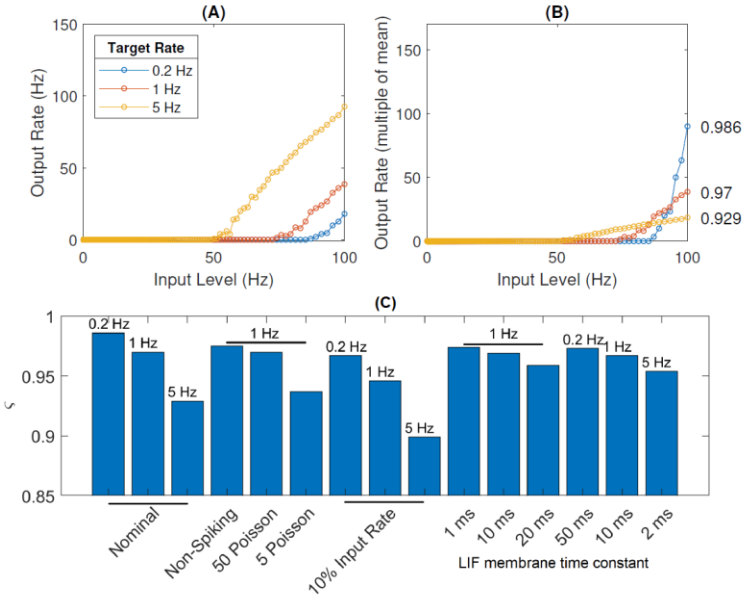

Figure 1. A single LIF neuron with a membrane time constant of 10 ms and spike-threshold chosen to achieve the given target rate (0.2 Hz, 1 Hz, or 5 Hz). Input is from 100 Poisson neuron inputs with rates varied logarithmically between 0.1 Hz and 100 Hz. (A) and (B) show the raw and scaled output spike rates as a function of input rates. The labels give the sparseness (ς) value for the 3 chosen target output spike rates. (C) Shows the sparseness (ς) values for a range of different parameter choices. The labels above each bar give the target spike rate. Labels below the bars are other parameter choices.

Acknowledgements
This work was supported by the Australian Research Council's Discovery Projects funding scheme [DP220101166].

References
1. Olshausen, B.A., Field, D.J.: **Sparse coding of sensory inputs.** Current Opinion in Neurobiology 14(4), 481–487 (Aug 2004).

ILIF: Temporal Inhibitory Leaky Integrate-and-Fire Neuron for Overactivation in Spiking Neural Networks

Kai Sun[1], Levin Kuhlmann[1], Peibo Duan[1],
[1] Department of Data Science and AI, Monash University, Australia.
E-mail: kai.sun1@monash.edu

The Spiking Neural Network (SNN) has drawn increasing attention for its energy-efficient, event-driven processing, and biological plausibility [1]. To train SNNs via backpropagation, surrogate gradients are used to approximate the non-differentiable spike function, but they only maintain nonzero derivatives within a narrow range of membrane potentials near the firing threshold—referred to as the surrogate gradient support width γ. We identify a major challenge, termed the dilemma of γ: a relatively large γ leads to overactivation [2], characterized by excessive neuron firing, which in turn increases energy consumption, whereas a small γ causes vanishing gradients and weakens temporal dependencies [3]. To address this, we propose a temporal Inhibitory Leaky Integrate-and-Fire (ILIF) neuron model, inspired by biological inhibitory mechanisms including hyperpolarization and retrograde inhibition [4] (see Figure 1). This model incorporates interconnected inhibitory units for membrane potential and current, effectively mitigating overactivation while preserving gradient propagation.

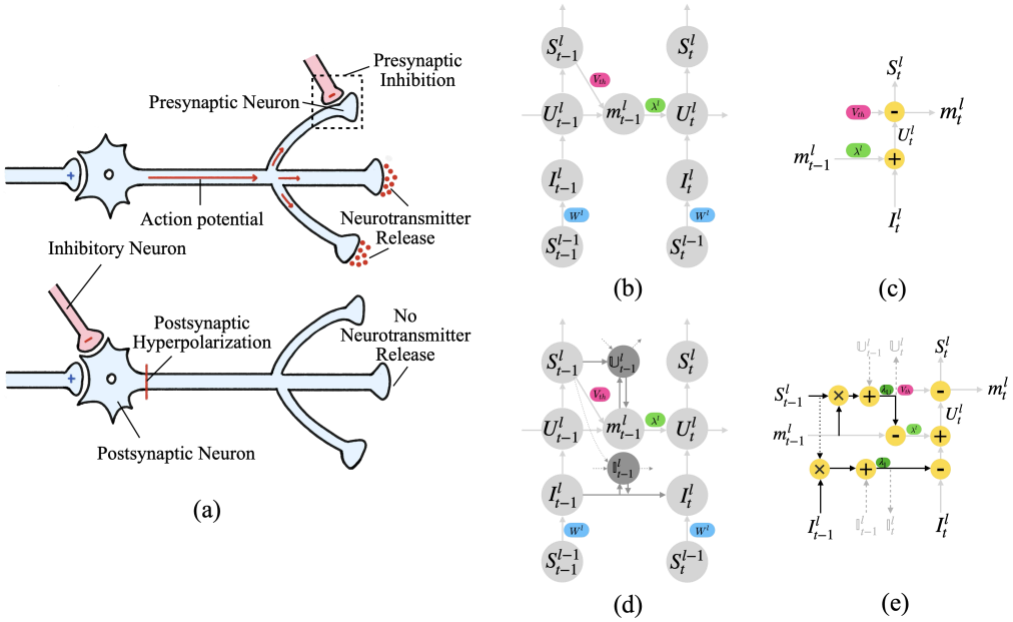

Figure 1. (a) Diagram of the inhibition mechanism, illustrating presynaptic inhibition and postsynaptic hyperpolarization.; (b) Structure of the vanilla LIF model; (c) Internal operations of the vanilla LIF model; (d) Structure of the ILIF model; (e) Internal operations of the ILIF model.

References

1. Schuman, Catherine D., et al.: **A Opportunities for neuromorphic computing algorithms and applications.** *Nature Nature Computational Science* 2022, 2.1: 10-19.
2. Niu, Li-Ye, and Ying Wei.: **Cirm-snn: Certainty interval reset mechanism spiking neuron for enabling high accuracy spiking neural network.** *Neural Processing Letters*, 2023, *55*(6), 7561-7582.
3. Huang, Yulong, et al.: **CLIF: Complementary Leaky Integrate-and-Fire Neuron for Spiking Neural Networks**. *Proceedings of the 41st International Conference on Machine Learning*, 2024, 235.
4. Bellec, Guillaume, et al.: **Long short-term memory and learning-to-learn in networks of spiking neurons**. *Advances in neural information processing systems*. 2018, 31.

Decoding visual perception from sheep visual cortex with temporal convolutional networks

Joel Villalobos[1,2], Stella Ho[1,2], Joseph West[3], Takufumi Yanagisawa[4], Weijie Qi[1,2], David Grayden[1,2], Sam John[1,2]
[1] Department of Biomedical Engineering, University of Melbourne, Victoria, Australia.
[2] Graeme Clark Institute for Biomedical Engineering, University of Melbourne, Victoria, Australia.
[3] Department of Computer Science, University of Melbourne, Victoria, Australia.
[4] Department of Neurosurgery, Graduate School of Medicine, Osaka University, Suita, Japan

E-mail: jvillalobos@unimelb.edu.au

Implantable neural interfaces enable recording of high-quality brain signals that can improve our understanding of brain function, while endovascular electrodes have a more manageable risk profile. This work aimed to use a minimally-invasive endovascular neural interface to record and interpret cortical activity from the visual cortex. We explored the use of temporal convolutional networks (TCN) to decode the visual cortical activity, as these models are presumed suitable for time-based signals.

A sheep model (n = 2) was used to record and decode visually evoked potentials from the cortex both with both endovascular and a subdural electrode grid (electrocorticography array). In awake animals, a series of 2 s visual stimuli were presented sequentially, consisting of a full-screen of colour (21" monitor) chosen between blue, green, cyan or white, interleaved with a blank screen for 0.4 s. The signals were sampled at 4.8 kHz and processed offline with a bandpass at 2–1000 Hz and notch at 50 Hz. Epochs of 2 s around stimulus onset were decoded using a TCN classifier with 5-fold cross-validation. A portion of the recordings (10%) was excluded during model training and validation and reserved for testing.

The accuracy of the 4-class TCN classifier was above 70% (see Figure 1) when using electrocorticography signals. Recordings exclusively from the ENI array resulted in lower decoding accuracy (40%) but were significantly above chance. This study is the first report of visually evoked neural activity using a minimally-invasive ENI.

Overall, the results show that implantable macro-electrodes yield sufficient spatial resolution to discern primary visual percepts from sheep cortex, using both endo-vascular and intracranial surgical placements. The TCN model was successful in classifying the time-domain signals without sub-sampling or

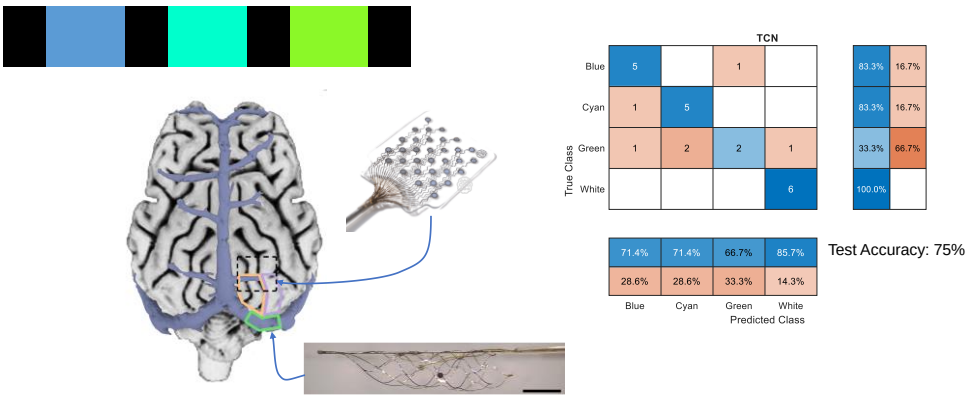

Figure 1. The visual cortex in sheep brain (left) was targeted with endovascular stent electrodes and an electrocorticography array and sequential visual stimuli of blue/green colour combinations were presented while awake. The TCN model used for decoding achieved test accuracy > 70%.

Acknowledgements
This research was funded by the Japan Science and Technology Agency's Moonshot Research and Development Program (JPMJMS2012). The studies were performed at the labs of the Florey Institute of Neuroscience and Mental Health, and the work relied on the support and contributions of Huakun Xin, Tom Vale, Quan Nguyen, Miranda Marcon and Prof. Yugeesh Lankadeva.

Making sense of attractor structure in human focal, generalized and induced seizures

Michaela Vranic-Peters[1], Patrick O'Brien[3], Udaya Seneviratne[3], Mark J. Cook[123], David B. Grayden[1], Andre Peterson[2]
[1] Department of Biomedical Engineering & Grame Clark Institute, University of Melbourne, Melbourne, Australia.
[2] Department of Medicine, University of Melbourne, Melbourne, Australia.
[3] St Vincent's Hospital Melbourne, Melbourne, Australia
E-mail: michaelap@student.unimelb.edu.au

Seizures can be distinguished by transitions of neural activity through pre-ictal, ictal, and post-ictal states, each associated with shifts in spectral power and phase coupling. Time-delay embedding allows the reconstruction of timeseries data in phase-space to create multi-dimensional attractors, whose geometric complexity can be quantified (Correlation Dimension D2) [1], and multi-scale stability can be assessed using scale-dependent Lyapunov exponents (SDLEs) [2]. These metrics originate from dynamical systems theory and require validation across diverse human datasets and seizure types, which demonstrate significant heterogeneity. Using EEG data from induced (photic, hyperventilation) and spontaneous seizures, and iEEG of focal seizures from the HUP database [3], we apply these metrics, and relate them to traditional measures including power spectra and phase-amplitude coupling (PAC). We find that generalised seizures (EEG) demonstrate a three-dimensional pseudo-cyclic attractor (see Figure 1), with reduced D2 (~2.2) compared to baseline (~2.5) associated with spectral red shift (power concentrates in low frequencies). In contrast, iEEG data of focal seizures display richer dynamics, with higher dimensional attractors (3-4D) and faster neural activity. Distributions of scale-dependent lyapunov exponents shift dramatically at each transition, suggesting a scale-dependence of seizure transition dynamics. Ranking iEEG channels by leading significant metric change could assist seizure onset zone localisation. All datasets showed faster post-ictal recovery compared to pre-ictal destabilization, often heralding reduced bandpower consistent with cortical depression. This work links attractor geometry to spectral dynamics, validating dynamical measures despite the variability demonstrated by clinical data. Robust metrics of state transitions can inform seizure prediction approaches and surgical epilepsy treatment.

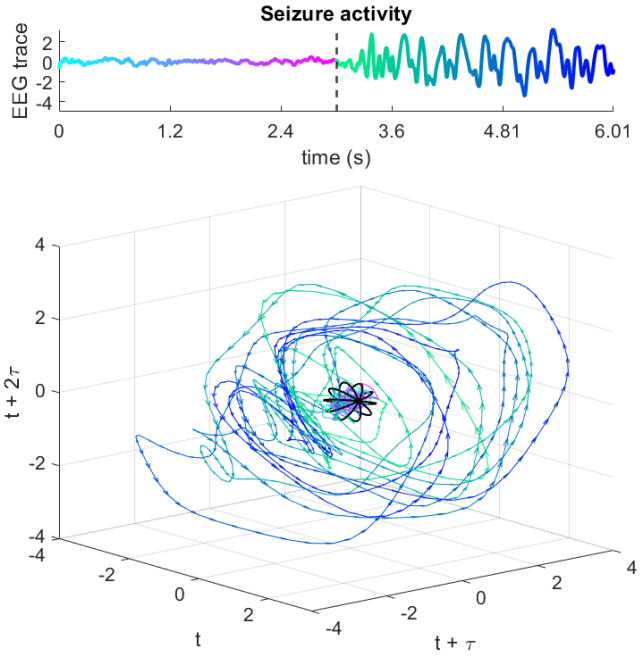

Figure 1. Timeseries data of EEG seizure activity (top) induced by photic stimulation initiating at the vertical dashed line, and corresponding attractor (bottom) obtained through time-delay embedding with a delay $\tau = 0.273$s and dimension = 3. Trajectory vector colour corresponds to timeseries data position. An ellipsoid marked with black rings encloses 99% of the pre-ictal data to illustrate a 'separatrix' or boundary. Axes units are normalized voltage.

References

1. Grassberger, P. and Procaccia, I., 1983. **Measuring the strangeness of strange attractors**. *Physica D: Nonlinear Phenomena*, *9*(1-2), pp.189-208.
2. Gao, J. B., et al., 2006. **Distinguishing chaos from noise by scale-dependent Lyapunov exponent.** *Physical Review E—Statistical, Nonlinear, and Soft Matter Physics* 74.6: 066204.
3. Bernabei, J.M., et al., (2023). **HUP iEEG Epilepsy Dataset**. *OpenNeuro*. [Dataset] doi: doi:10.18112/openneuro.ds004100.v1.1.3

Single-Spike Spatial Learning and Spatio-Temporal Optimisation in Spiking Autoencoders

Ben Walters[1], Yeshwanth Bethi[2], Hamid Rahimian Kalatehbali[3], Amirali Amirsoleimani[3], Saeed Afshar[2], Mostafa Rahimi Azghadi[1],
[1] College of Science and Engineering, James Cook University, Townsville, Australia.
[2] International Center for Neuromorphic Systems, Western Sydney University, Sydney, Australia
[3] Department of Electrical Engineering and Computer Science, York University, Toronto, Canada
E-mail: mailto:ben.walters@my.jcu.edu.au

Spiking Neural Networks (SNNs) offer a low-power alternative to traditional deep neural networks, leveraging their sparse, event-driven nature for efficient processing of static and event-based data. While previous spiking auto-encoders were power-hungry and limited to static data, this presentation introduces a novel architecture for efficient and high-quality reconstruction of both static and spatiotemporal data, as shown in Figure 1. We demonstrate that our hidden layer can encode each static input with a single spike, minimizing power consumption. Additionally, our modified decoder neuron model enables precise control over output spike timing, leading to improved reconstruction quality. We validate our spatiotemporal reconstructions on the Spiking Heidelberg Digits (SHD) dataset, exploring the trade-off between spike count and reconstruction accuracy. Our findings pave the way for complex SNNs to operate more efficiently.

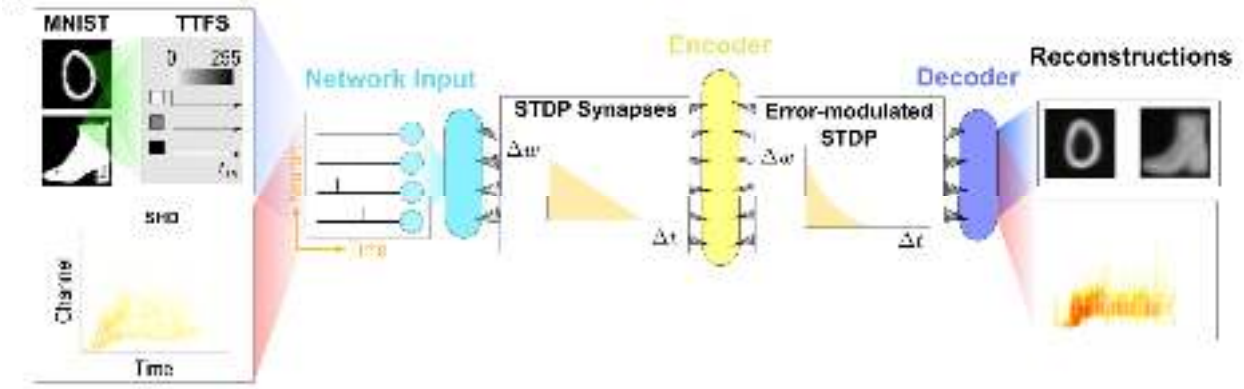

Figure 1. Spiking autoencoder architecture for static and spatio-temporal input reconstruction.

Acknowledgements
We would like to acknowledge the Research Training Program (RTP) scholarship and the JCU competitive research training grant for funding this research.

Exploring Brain Criticality as a Potential Biomarker for Depression

Han Wang[1], Young Jun Jung[2], Steven Prawer[1], Michael Ibbotson[2], Wei Tong[1].
[1] School of Physics, University of Melbourne, VIC, Australia
[2] Department of Biomedical Engineering, University of Melbourne, VIC, Australia
Email: hww9@student.unimelb.edu.au

Depression is a prevalent disorder that significantly impairs emotional well-being and daily life causing social isolation and economic hardship, and a substantial loss of quality of life [1]. Identifying reliable biomarkers is essential for advancing personalized treatment strategies. According to brain criticality theory, the brain operates near a critical state, with deviations from this state proposed as potential indicators of neurological and neuropsychiatric diseases, such as epilepsy [2]. In this study, we explore the potential of brain criticality as a biomarker for depression using electrophysiology recordings.

Multi-channel electrode recordings were performed in the hippocampus of two groups of C57BL/6 mice: corticosterone-treated (CORT) and wild-type control (CON). CORT mice show depression-like behaviours and have been widely used as an animal model of depression [3]. Recordings were conducted while the animals were under anesthesia, both pre- and post- injection of the antidepression drug, sertraline, as shown in Figure 1.a. Branching ratio, a main measure of brain criticality, was estimated using a multistep regressive estimator [4]. The coefficient of variation of the branching ratio was evaluated to assess the variability of brain network dynamics.

The branching ratio differed significantly between the CORT and CON groups after sertraline was applied ($p<0.05$), as shown in Figure 1.b. The coefficient of variation of the branching ratio was higher in CORT mice, as shown in Figure 1.c, although statistical significance was not achieved, likely due to the small sample size. These results suggest that the branching ratio is a promising biomarker for depression and antidepressant response. Furthermore, these findings provide valuable insights for developing real-time brain activity monitoring devices to optimize depression treatment.

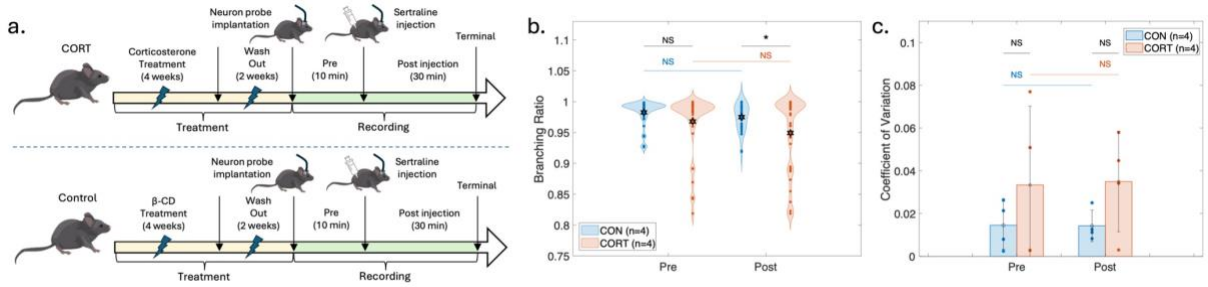

Figure 1. a. Schematic of experimental design and multi-channel electrode recordings. b. Box plots of branching ratios of corticosterone-treated (CORT) and control (CON) groups pre and post injection of sertraline. Stars represent the mean values. c. Bar plots showing the mean coefficient of variation of the branching ratios, with error bars representing the standard deviation, in the animals pre and post sertraline. NS: no significant difference, *: p-value<0.05.

Acknowledgements
HW is supported by the Australian Government Research Training Program (RTP) Scholarship and the Graeme Clark Institute (GCI) Top-up Scholarship. This study was supported by a GCI Internal Seed Fund.

Reference
1. Smith, K. **Mental health: A world of depression.** Nature 515, 180–181 (2014).
2. Corsi, MC., et al. **Neuronal avalanches in temporal lobe epilepsy as a noninvasive diagnostic tool investigating large scale brain dynamics.** Sci Rep 14, 14039 (2024).
3. Berger, S., et al. **Effect of Chronic Corticosterone Treatment on Depression-Like Behavior and Sociability in Female and Male C57BL/6N Mice.** Cells, 8(9), 1018 (2019).
4. Wilting, J., Priesemann, V. **Inferring collective dynamical states from widely unobserved systems.** Nat Commun 9, 2325 (2018).

Investigating cortical visual prosthesis with realistic computer simulations

Haozhe Zac Wang[1], Yan Tat Wong[1,2],
[1] Department of Electrical and Computer System Engineering, Monash University, Australia
[2] Department of Physiology, Monash University, Australia
E-mail: haozhe.wang1@monash.edu

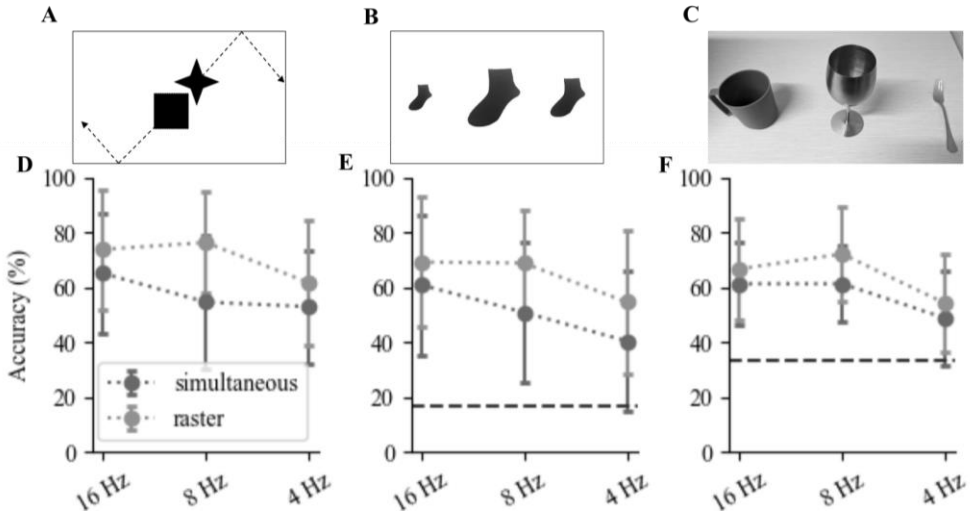

Figure 1- A-C) Example of dynamic shape recognition, sorting, dining table recognition. D-F) Participants' accuracy for each task.

Cortical visual prostheses restore vision by stimulating neurons in the early visual cortex, evoking bright dots in the visual field known as phosphenes. Despite the advancement of this technology, simultaneously stimulating multiple electrodes may cause complications in visual perception, such as phosphene distortion [1]. Moreover, this could overflow the brain with excessive charges. Alternatively, we could dynamically evoke phosphene via current steering, where a single phosphene moves smoothly to represent simple visual stimuli, such as letters [2].

We proposed a new stimulation protocol called "raster scanning" to combine the strength of both methods. We activated a small number of phosphenes per frame and sequentially activated them to present the outline of complex objects. Due to the risk of neurosurgeries, we simulated the resulting vision on an HTC VIVE VR headset with an MRI-derived phosphene map [3]. We recruited twenty participants to evaluate the efficiency of raster scanning against simultaneous presentation. We estimated both methods under three refresh rates: 4Hz, 8, and 16Hz. We ran three psychophysics tasks to assess participants' visual performance: dynamic shape recognition, sorting, and dining table recognition. We hypothesise that raster scanning would perform better at static recognition tasks but not fast-localisation tasks.

We found that raster scanning improved participants' accuracy and reduced response time for all three tasks. In addition, raster scanning could also reduce head movement for dynamic shape recognition and dining table recognition tasks. Our results highlight the potential for using raster scanning in cortical prosthetic vision in the future. This method could be a more efficient and safer way to convey visual information. We believe more sessions might help us understand how participants adapt to this new stimulation protocol and further optimise this method.

References

1. E. Fernández et al. **Visual percepts evoked with an Intracortical 96-channel microelectrode array inserted in human occipital cortex.** Journal of Clinical Investigation 2021, 131(23):e151331.

2. M. S. Beauchamp et al. **Dynamic stimulation of visual cortex produces form vision in sighted and blind humans.** Cell 2020, 181(4):774-783.e5.

3. H. Z. Wang and Y. T. Wong **A novel simulation paradigm utilising MRI-derived phosphene maps for cortical prosthetic vision.** Journal of Neural Engineering 2023, 10;20(4):046027.

Primary visual cortex model to examine post-stimulation suppression

Jessica F. Woolley[1], Sabrina J. Meikle[1,2], Nicholas S.C. Price[2], Yan T. Wong[1,2],
[1] Department of Electrical and Computer Systems Engineering, Monash University, Clayton, VIC, Australia
[2] Department of Physiology and Biomedicine Discovery Institute - Neuroscience Program, Monash University, Clayton, VIC, Australia.
E-mail: jessica.woolley@monash.edu

Cortical visual prostheses aim to restore sight for the legally blind by directly stimulating the brains visual cortex with electricity which can cause the perception of spots of light, used to build desired images. A current limitation is post-stimulation suppression (PSS), where after stimulation activity of tissue surrounding the electrodes reduces [1]. Computational modelling of the brain has been used to explore PSS, linking it to both individual cell factors and feedforward/feedback inhibitory synapses [1], but did not include connections between stimulated cells. We hypothesize that changes to the connection strengths which include inhibitory cells will modify the duration of PSS.

We have created, with the Brain Machine Toolkit [2], a model of layer 2/3 in the primary visual cortex (V1) with 1066 cells (80% excitatory) using connection to a 1000 sp/s Poisson cell (baseline) for baseline spike rate. A new method to model stimulation has been developed to allow simulation of cells close to the electrode. The connection strength between cells (excitatory/excitatory (EE), excitatory/inhibitory (EI), inhibitory/excitatory (IE), inhibitory/inhibitory (II), baseline/ excitatory (BE), baseline/inhibitory (BI)) has been optimized to match stimulation of V1 in a rat, collected by our group [3]. For optimization 10µA of current was used to maximize activated cells for calculating PSS, and final accuracy was determined across a range of currents (1.5µA,2.5µA,4µA, 5µA,7.5µA). To determine connection impact on PSS the magnitude of the optimized strength of was scaled (0x,0.001x,0.1x,10x,100x) for all types.

The optimized model was not statistically significantly different from experiment (Spiking rate = model: 5±10sp/s, experiment: 5±5sp/s, p=0.89; PSS = model: 45±7ms, experiment: 45±2ms, p=0.87; mean±sd, unpaired t-test). When the optimized connection strengths were scaled there was no significant change for any reduction in magnitude or increase for IE, II, BE, EI or BI which opposes the hypothesis. However, there was a significant decrease in PSS as the magnitude increased for EE (10x = 37±13ms, p=0.017; 100x = 11±10ms, p=0.0001; mean±sd, unpaired t test). As there was no change for when the connection was removed (0x) this supports previous results indicating a cellular component of PSS. The reduction of PSS with high excitatory connections may be due to loss of stability in the network, indicating PSS may be important in maintaining network stability during sudden peaks of activity.

References

1. Kumaravelu K., and Grill W.M.: **Neural mechanisms of the temporal response of cortical neurons to intracortical microstimulation.** *Brain Stim* 2024, 17(2), 365-381.
2. Dai, K. and et al.: **Brain Modeling ToolKit: An open source software suite for multiscale modeling of brain circuits**. *PLoS Comp Bio*. 2020, 16(11).
3. Meikle S.J., Hagan M.A., Price N.S.C. and Wong Y.T.: **Intracortical current steering shifts the location of evoked neural activity.** *J Neural Eng*. 2022, 19(3).

Age-Related Structural Brain Changes Drive Shifts in Intrinsic Timescales and Neural Dynamics

Kaichao Wu[1,2], Leonardo Gollo[1,2,3]
[1] The Turner Institute for Brain and Mental Health, Monash University, Australia.
[2]Monash Biomedical Imaging, Monash University, Australia.
[3] Instituto de Física Interdisciplinary Sistemas Complejos, IFISC (UIB-CSIC), Spain
E-mail: kaichao.wu@monash.edu

Intrinsic timescales of brain regions exhibit heterogeneity and are crucial for the temporal integration of external stimuli[1,2]. Aging, often associated with cognitive decline, leads to neuronal and synaptic loss, reshaping brain structure and dynamics[3]. However, the impact of these structural changes on temporal coding in the aging brain remains unclear. We mapped intrinsic timescales and gray-matter volume (GMV) using MRI in young and elderly adults. Elderly subjects showed shorter intrinsic timescales across functional networks and a positive association between timescales and GMV. Using an age-dependent spiking neuronal network model[4,5], we found younger brains near a critical branching regime, while aging pushed dynamics toward a subcritical state. This shift explains reduced intrinsic timescales and highlights structural changes driving altered brain dynamics, offering insights into cognitive decline interventions.

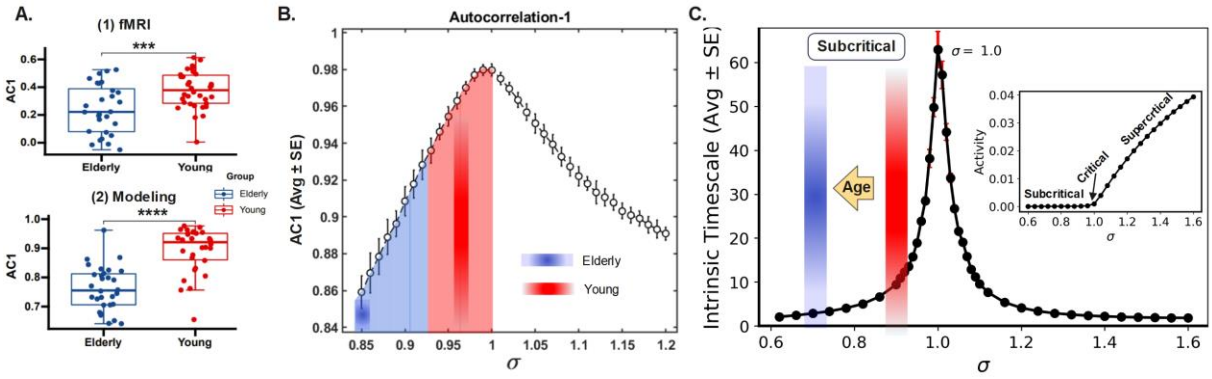

Figure 1. Brain networks in elderly subjects show a greater distance to criticality. A. Autocorrelation with lag 1 (AC1) for fMRI BOLD timeseries (top) and neuronal network modeling (bottom). B. AC1 peaks at the critical branching ratio (σ_c =1). The branching ratio (σ) quantifies the propagation of activity between neurons: $\sigma < 1$ indicates a subcritical state with reduced activity spread, $\sigma = 1$ reflects criticality with balanced propagation, and $\sigma > 1$ represents a supercritical state with excessive activity spread. (C) Intrinsic timescales peak at $\sigma = 1$, with aging shifting the network toward subcriticality ($\sigma<1$, yellow arrow). Inset: Neuronal network phase transition occurs at $\sigma_c = 1$.

Acknowledgements
This work was supported by the Australian Research Council (ARC), Future Fellowship (FT200100942), the Rebecca L. Cooper Foundation (PG2019402), the Ramón y Cajal Fellowship (RYC2022-035106-I) from FSE/Agencia Estatal de Investigación (AEI), Spanish Ministry of Science and Innovation, and the María de Maeztu Program for units of Excellence in R&D, grant CEX2021-001164-M.

References

1. Murray, John D., et al. "A hierarchy of intrinsic timescales across primate cortex." *Nature neuroscience* 17.12 (2014): 1661-1663.
2. Watanabe, Takamitsu, Geraint Rees, and Naoki Masuda. "Atypical intrinsic neural timescale in autism." *Elife* 8 (2019): e42256.
3. Morrison, John H., and Mark G. Baxter. "The ageing cortical synapse: hallmarks and implications for cognitive decline." *Nature Reviews Neuroscience* 13.4 (2012): 240-250.
4. Wu, Kaichao, and Leonardo Lyra Gollo. "Mapping and Modeling Age-Related Changes in Intrinsic Neural Timescales." *Communication Biology* (2025): 2024-09. https://doi.org/10.1038/s42003-025-07517-x
5. Kinouchi, Osame, and Mauro Copelli. "Optimal dynamical range of excitable networks at criticality." *Nature physics* 2.5 (2006): 348-351

Simulating Psychophysical Forward Masking in a User-Specific Model of a Cochlear Implant

Xiaowei Xia[1], Demi X. Gao[2,3], Martin Spencer[1], Tim Brochier[4], David B. Grayden[1,2]
[1] Department of Biomedical Engineering and Graeme Clark Institute, The University of Melbourne, Australia.
[2] Bionics Institute, Australia.
[3] Department of Medical Bionics, The University of Melbourne, Australia.
[4] Cochlear Limited, Australia.
E-mail: xiaowei.xia@student.unimelb.edu.au

The Cochlear Implant (CI) provides hearing to individuals with hearing loss by directly stimulating auditory nerve fibres (ANFs). Spread of excitation from stimulated electrodes can vary significantly between users, directly impacting their hearing performance. Psychophysical Forward Masking (PFM) measures the increase in the detection threshold of a probe when presented after a masker [1] to estimate the extent of spread of excitation of electric fields from electrodes and the potential impact upon the ability to perceive nearby electrodes. While it is known that PFM involves processes more central than the auditory nerve [2], the underlying mechanism remains unclear. This research aims to develop a model to explain these mechanisms using a user-specific computational model and PFM data. Data from previous PFM experiments with CI recipients [1] were used to obtain user-specific information, including masker and probe positions, current levels and masking profiles. With a masker stimulation of 300 ms duration at 250 pulses/s on a fixed electrode position at 80% of dynamic range, the masking profile shows how many additional current levels in a subsequent probe stimulus (20 ms, 250 pulses/s) are required to perceive the probe.

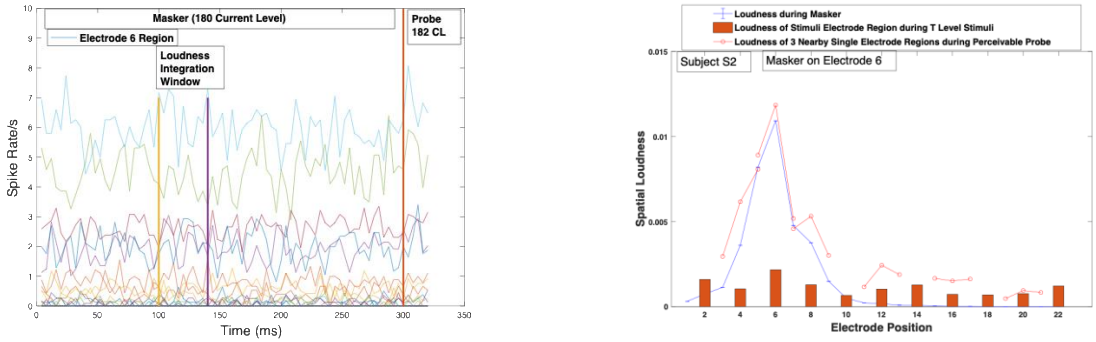

(a) (b)

Figure 1 (a) An example of neural activations in different regions of the cochlea during masker (300 ms pulse train on electrode 6, 250 pulses/s) and probe (20 ms pulse train on electrode 6) after applying a loudness integration window. (b) Simulation plots of one CI user for one masker position and different probe positions.

To study the additional neural activation required to perceive the probe, we used an existing stochastic neural model [3] to obtain neural activations of the masker and probe. The neural activity of 100 ANFs in the model at each electrode position was integrated over a 40 ms moving window to estimate perceived spatial loudness, as shown in Figure 1(a). Spatial loudness is presented by the neural spikes in each electrode region divided by the total number of ANFs. The neural spikes and spatial loudness at each probe location during unmasked threshold level stimulation were also obtained. Figure 1(b) shows an example simulation of a CI recipient's activated ANFs at different electrode positions during the masker (blue curves), perceivable probes (red curves) and unmasked threshold stimulation (orange bars) for one masker position and different probe positions. In future research, the criteria of a probe being detected will be determined to improve the accuracy of the simulation results.

References

[1] L. T. Cohen, E. Saunders, M. R. Knight, and R. S. C. Cowan, "Psychophysical measures in patients fitted with Contour™ and straight Nucleus electrode arrays," *Hear. Res.*, vol. 212, no. 1, pp. 160–175, Feb. 2006.
[2] R. V. Shannon, "Forward masking in patients with cochlear implants," *J. Acoust. Soc. Am.*, vol. 88, no. 2, pp. 741–744, Aug. 1990.
[3] I. C. Bruce *et al.*, "A stochastic model of the electrically stimulated auditory nerve: single-pulse response," *IEEE Trans. Biomed. Eng.*, vol. 46, no. 6, pp. 617–629, Jun. 1999, doi: 10.1109/10.764938.

Leveraging Temporal Neural Dynamics for Forecasting Seizure Duration Using a Neural Mass Model and Random Forests

Parvin Zarei Eskikand[1,2], Mark J. Cook[1,2,3], Anthony N. Burkitt[1,2], David B. Grayden[1,2,3]
[1] Department of Biomedical Engineering, The University of Melbourne, Victoria, Australia
[3] Graeme Clark Institute for Biomedical Engineering, The University of Melbourne, Victoria, Australia.
[3] Department of Medicine, St Vincent's Hospital, Melbourne, Victoria, Australia
E-mail: pzarei@unimelb.edu.au

Understanding the temporal dynamics of seizures offers valuable insights into the underlying neurophysiological mechanisms associated with epileptic events. The duration of seizures is a fundamental aspect that reflects the severity and impact of the epileptic condition on the brain. To explore this, we developed a Neural Mass Model (NMM) for a cortical column, comprising interconnected motifs representing layers 2/3, 4, and 5 of the cortex. Each motif includes excitatory and inhibitory neuron populations interconnected through forward and recurrent inhibitory and excitatory connections [1]. We fitted the connectivity weights in the NMM to the intracranial EEG (iEEG) data from a Tetanus Toxin rat model of epilepsy [2, 3].

Our investigation aims to understand how model parameters change with the duration of seizures. Seizures in the first quantile of the duration distribution for individual rats were classified as short seizures, while those in the last quantile were classified as long seizures. A Random Forest classification algorithm was employed to distinguish between the two classes. The Random Forest model was trained using connectivity strength values from the NMM, specifically the connectivity one minute before seizures and the average connectivity strength during the first five seconds following seizure onset. Bayesian optimization was utilized to fine-tune the model's hyperparameters, and feature importance scores were calculated to identify the most relevant features for classification. The classifier was retrained using the selected features to enhance its performance. Model evaluation was performed using the Area Under the Receiver Operating Characteristic Curve (AUC), providing insights into the trade-off between sensitivity and specificity.

The Random Forest classifier demonstrated robust performance in distinguishing between long and short seizures. When using connectivity strength values from the NMM model one minute before seizure onset and during the first five seconds of the seizure, the classifier achieved a high AUC=0.91, indicating strong sensitivity and specificity. In comparison, the performance of the classifier trained solely on connectivity strength values from one minute before seizure onset showed a slight decrease in AUC=0.70, suggesting that incorporating features from the seizure onset period enhances the model's discriminative power

These findings highlight the importance of combining pre-seizure and early seizure dynamics for classifying seizure duration. The results suggest that the neural network parameters during seizure initiation provide complementary information to pre-seizure connectivity, thereby improving classification accuracy. This underscores the value of leveraging temporal changes in neural dynamics for understanding and predicting seizure characteristics, which could inform personalized therapeutic interventions and seizure forecasting.

Acknowledgment

This work was funded by the Australian Government under the Australian Research Council's Training Centre in Cognitive Computing for Medical Technologies (IC170100030).

References

[1] Zarei Eskikand PZ, Soto-Breceda A, Cook MJ, Burkitt AN, Grayden DB. **Inhibitory stabilized network behaviour in a balanced neural mass model of a cortical column.** Neural Networks. 2023 Sep 1;166:296-312.

[2] Crisp DN, Cheung W, Gliske SV, Lai A, Freestone DR, Grayden DB, Cook MJ, Stacey WC. **Quantifying epileptogenesis in rats with spontaneous and responsive brain state dynamics.** Brain Communications. 2020;2(1):fcaa048.

[3] Freestone DR, Karoly PJ, Nešić D, Aram P, Cook MJ, Grayden DB. **Estimation of effective connectivity via data-driven neural modeling.** Frontiers in neuroscience. 2014:383.